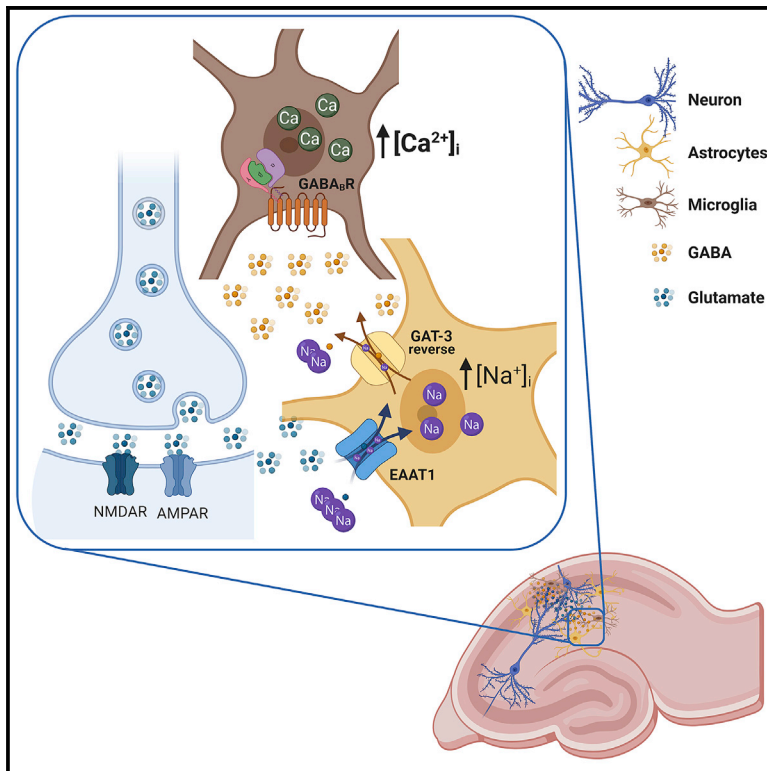


# Microglia sense neuronal activity via GABA in the early postnatal hippocampus

## Graphical abstract



## Authors

Francesca Logiacco, Pengfei Xia, Svilen Veselinov Georgiev, ..., Ralf Kühn, Helmut Kettenmann, Marcus Semtner

## Correspondence

marcus.semtner@mdc-berlin.de

## In brief

Logiacco et al. generate microglia-specific calcium indicator mice. Using acute brain slices, they demonstrate that neuronal stimulation of the Schaffer collateral pathway evokes intracellular  $\text{Ca}^{2+}$  responses in the microglia that depend on astrocytic GABA, glutamate transporters, and microglial  $\text{GABA}_B$  receptors.

## Highlights

- Microglia respond to Schaffer collateral stimulation in the neonatal hippocampus
- Responses depend on microglial  $\text{GABA}_B$ Rs and astrocytic glutamate and GABA transporters
- Lack of responses in adults may be due to developmental changes in astrocyte physiology



## Article

# Microglia sense neuronal activity via GABA in the early postnatal hippocampus

Francesca Loggiacco,<sup>1,2</sup> Pengfei Xia,<sup>1</sup> Svilen Veselinov Georgiev,<sup>1</sup> Celeste Franconi,<sup>1</sup> Yi-Jen Chang,<sup>1</sup> Bilge Ugursu,<sup>1,3</sup> Anje Sporbert,<sup>5</sup> Ralf Kühn,<sup>4</sup> Helmut Kettenmann,<sup>1,6,7</sup> and Marcus Semtner<sup>1,7,8,\*</sup>

<sup>1</sup>Cellular Neurosciences, Max-Delbrück-Center for Molecular Medicine in the Helmholtz Association, 13125 Berlin, Germany

<sup>2</sup>Department of Biology, Chemistry, and Pharmacy, Freie Universität Berlin, 12169 Berlin, Germany

<sup>3</sup>Experimental Ophthalmology, Charité Universitätsmedizin Berlin, Augustenburger Platz 1, 13353 Berlin, Germany

<sup>4</sup>Transgenic Core Facility, Max-Delbrück-Center for Molecular Medicine in the Helmholtz Association, 13125 Berlin, Germany

<sup>5</sup>Advanced Light Microscopy, Max-Delbrück-Center for Molecular Medicine in the Helmholtz Association, 13125 Berlin, Germany

<sup>6</sup>Shenzhen Institutes of Advanced Technology, Chinese Academy of Sciences, Shenzhen, China

<sup>7</sup>These authors contributed equally

<sup>8</sup>Lead contact

\*Correspondence: [marcus.semtner@mdc-berlin.de](mailto:marcus.semtner@mdc-berlin.de)

<https://doi.org/10.1016/j.celrep.2021.110128>

## SUMMARY

Microglia, the resident macrophages in the central nervous system, express receptors for classical neurotransmitters, such as  $\gamma$ -aminobutyric acid (GABA) and glutamate, suggesting that they sense synaptic activity. To detect microglial  $\text{Ca}^{2+}$  responses to neuronal activity, we generate transgenic mouse lines expressing the fluorescent  $\text{Ca}^{2+}$  indicator GCaMP6m, specifically in microglia and demonstrate that electrical stimulation of the Schaffer collateral pathway results in microglial  $\text{Ca}^{2+}$  responses in early postnatal but not adult hippocampus. Preceding the microglial responses, we also observe similar  $\text{Ca}^{2+}$  responses in astrocytes, and both are sensitive to tetrodotoxin. Blocking astrocytic glutamate uptake or GABA transport abolishes stimulation-induced microglial responses as well as antagonizing the microglial GABA<sub>B</sub> receptor. Our data, therefore, suggest that the neuronal activity-induced glutamate uptake and the release of GABA by astrocytes trigger the activation of GABA<sub>B</sub> receptors in microglia. This neuron, astrocyte, and microglia communication pathway might modulate microglial activity in developing neuronal networks.

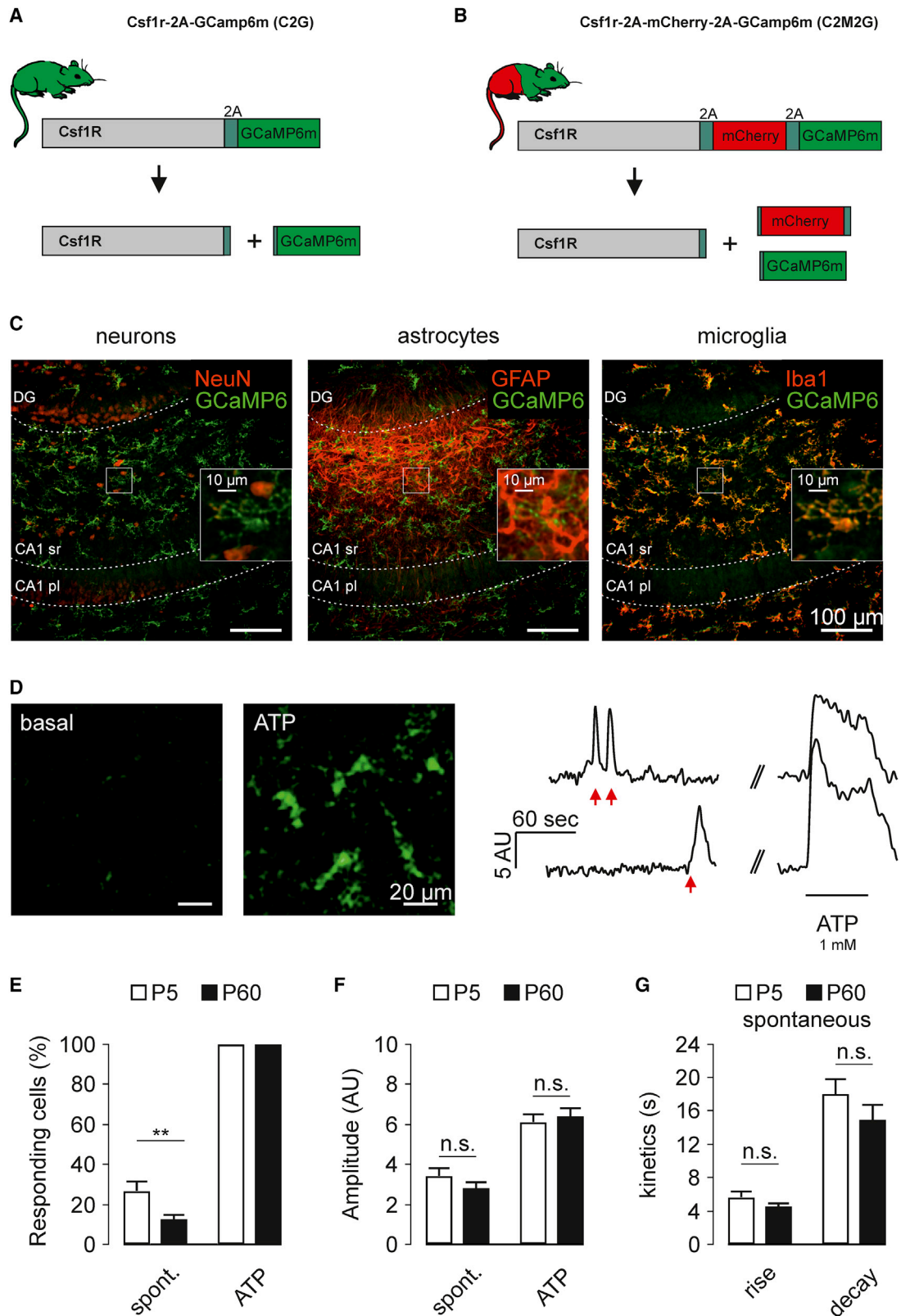
## INTRODUCTION

Microglia are an integral part of the brain's cellular network and modulate neuronal homeostasis and development (Kettenmann et al., 2013; Michell-Robinson et al., 2015). Synaptic connections in rodents are established during the early neonatal phase (Ben-Ari et al., 2007), in which synapses are initially overproduced, leading to pruning in an activity-dependent fashion (Chechik et al., 1998). Microglia constantly scan their environment, with their fine processes extending and retracting at a rate of few micrometers per minute (Davalos et al., 2005; Nimmerjahn et al., 2005). Recent evidence indicates that microglial processes are directed toward neuronal axons and dendrites, in which they are implicated in monitoring and regulating neuronal activities (Tremblay et al., 2011; Pascual et al., 2012; Kettenmann et al., 2013; Schafer et al., 2013; Wake et al., 2013), including their involvement in the formation and pruning of synapses (Paolicelli et al., 2011; Miyamoto et al., 2016). Physical interactions of microglia with synapses as well as the developmental pruning of afferent inputs depend on neural activity (Wake et al., 2009; Schafer et al., 2012). Complement factors have an important role in neuron-microglia signaling (Schafer et al., 2012), but that is likely not the only pathway. One intriguing option would be that micro-

glia detect the spillover of neurotransmitters originating from synaptic release during neurotransmission. Such a communication pathway is already established for astrocytes, which sense neurotransmitter release via a large repertoire of neurotransmitter receptors and transporters that enables them to detect and control the activity of the surrounding neuronal network. In turn, astrocytes are able to respond to neuronal activity by releasing gliotransmitters, such as glutamate, ATP, adenosine, D-serine (Haydon and Carmignoto, 2006; Panatier et al., 2006; Volterra and Meldolesi, 2005), and  $\gamma$ -aminobutyric acid (GABA) (Angulo et al., 2008), thereby feeding back on the neuronal network.

Microglia are equipped with a plethora of classical neurotransmitter receptors, such as those for purines, GABA, or glutamate (Pocock and Kettenmann, 2007; Kettenmann et al., 2011). Microglia express ionotropic receptors, such as P2X receptors, but most microglial receptors are G-protein-coupled receptors and, therefore, elicit, upon activation, cytosolic  $\text{Ca}^{2+}$  elevations from internal stores by phospholipase C (PLC) activation via the  $\text{G}\alpha\text{q}$  protein and/or the  $\text{G}\beta\gamma$  complex (Clapham, 2007; Mariotti et al., 2016). Indeed, the functional expression of such neurotransmitter receptors, including GABA<sub>B</sub> (Kuhn et al., 2004; Favuzzi et al., 2021), histamine, dopamine (Pannell et al.,





(legend on next page)

2014), serotonin (Krabbe et al., 2012), and muscarinic acetylcholine receptors (Pannell et al., 2016), was previously demonstrated by live-cell  $\text{Ca}^{2+}$  imaging techniques on freshly isolated microglia or neonatal and adult primary cultures. It also became evident that only a subpopulation of microglia responds to a given neurotransmitter, implying a large heterogeneity in their chemosensitivity. Recent evidence suggests that neuronal activity is sensed by microglia (Umpierre et al., 2020; Umpierre and Wu, 2020; Liu et al., 2021), raising the possibility that intrinsic neurotransmitter receptors enable microglia to sense synaptic activity. An experimental approach characterizing microglial  $\text{Ca}^{2+}$  responses triggered by neurotransmitters *in situ* and *in vivo* would require an experimental model that robustly monitors microglial  $\text{Ca}^{2+}$  elevations, such as a mouse model expressing a genetically encoded  $\text{Ca}^{2+}$  indicator (GECI) specifically in microglia at developmental and adult stages. Although various groups approached microglial  $\text{Ca}^{2+}$  recordings *in situ* and *in vivo*, there were always disadvantages in the models, including the potential microglia activation after virus injection (Seifert et al., 2011; Brawek et al., 2017) or single-cell electroporation (Eichhoff et al., 2011), as well as low microglia specificity of the available Cre mouse lines, such as Iba1-Cre or CX3CR1-Cre, leading to leaking expression of the  $\text{Ca}^{2+}$  sensor in cortical and hippocampal neurons (Gee et al., 2014; Pozner et al., 2015). In the present study, we generated a microglia  $\text{Ca}^{2+}$  indicator mouse model that works independently of the Cre recombinase activity or viruses. Microglia-specific expression of the genetically encoded  $\text{Ca}^{2+}$  indicator GCaMP6m was achieved by insertion of the expression cassette and a self-cleaving 2A linker immediately before the stop codon of the endogenous *Csf1r* gene. This mouse model enabled us to reliably monitor  $\text{Ca}^{2+}$  level changes in microglia from neonatal and adult hippocampal brain slices after Schaffer collateral stimulation, and we provide evidence for a complex neuron, astrocyte, microglia communication pathway, which enables microglia to indirectly sense neuronal activity.

## RESULTS

### C2G and C2M2G $\text{Ca}^{2+}$ indicator mouse lines express GCaMP6m in microglia specifically

We generated two mouse lines—*Csf1r*-2A-GCaMP6m (C2G) and *Csf1r*-2A-mCherry-2A-GCaMP6m (C2M2G)—that express the  $\text{Ca}^{2+}$  indicator protein GCaMP6m in microglia specifically (see Method details and Figures 1A and 1B). For validation of

these mouse models, brain slices from P5–6 mice were immunolabeled with antibodies against GFP (targeting GCaMP6m), combined with staining against mCherry and Iba-1 (targeting microglia). As shown in Figure 1C, the hippocampal GCaMP6m signal was expressed in the somata and processes of nearly all Iba1<sup>+</sup> cells of C2G and C2M2G mice (Figure 1C). No signals were found in the neurons and astrocytes, indicating the specificity of GCaMP6m expression in microglia. Highly microglia-specific GCaMP6m expression was also found among other gray (cortex, striatum, and cerebellum) and white (corpus callosum) matter brain regions in neonatal and adult C2G and C2M2G mice (Figures S1 and S2). Quantification of the stainings of C2G and C2M2G hippocampal brain slices at P5–6 demonstrated that 98.4% ± 0.4% of the GCaMP6m<sup>+</sup> cells were Iba-1<sup>+</sup>, whereas 95.1% ± 0.8% of Iba-1<sup>+</sup> cells were GCaMP6m<sup>+</sup> throughout all investigated brain regions, indicating the successful development of microglia-specific GCaMP6m mouse lines labeling nearly all microglia and displaying no abundant expression in other cell types than microglia. We performed *in situ*  $\text{Ca}^{2+}$  imaging recordings in hippocampal brain slices from neonatal (P5–6) and adult (P45–70) mice using two-photon live-cell imaging. The intensity of the GCaMP6m fluorescence under basal conditions was very low in both mouse models, and microglia were nearly indistinguishable from background fluorescence (Figure S3). Considering the rather low  $K_D$  of GCaMP6m for  $\text{Ca}^{2+}$  (164 ± 31 nM; Barnett et al., 2017), we conclude from these control experiments that basal  $\text{Ca}^{2+}$  levels in microglia must be very low. In accordance to previous observations *in vitro* (Korvers et al., 2016) and *in vivo* (Brawek et al., 2014; Eichhoff et al., 2011), we found resting  $\text{Ca}^{2+}$  levels in microglia somata were spontaneously interrupted by transient elevations in a subset of the recorded cells (Figure 1D). Thus, at P5–6, 26.6% ± 4.9% (n = 8 mice, 17 slices, 406 cells) of the microglia displayed these events during a recording time of 5 min. The frequency was 10.1 ± 2.8 events/cell and per hour. These spontaneous events had rise and decay times of 5.6 ± 0.7 s and 18.0 ± 1.8 s, respectively. In adult brain slices, spontaneous microglial  $\text{Ca}^{2+}$  elevations also occurred; however, in a significantly lesser percentage of cells (12.2% ± 2.1%; n = 5 mice, 19 slices, 577 cells; p = 0.0079) but with similar properties (4.5 ± 0.4 s for rise times, p = 0.1860; 14.9 ± 1.8 s for decay times, p = 0.2455) as in neonatal microglia (Figures 1E–1G). The frequency was significantly less than that in neonatal microglia (2.6 ± 0.6 events/cell and per hour; p = 0.0061). There were no significant differences in

### Figure 1. C2G and C2M2G mice express GCaMP6m specifically in microglia

(A and B) Transgenic strategy used for microglia-specific GCaMP6m expression in the mouse lines 2A-GCaMP6m (C2G) (A) and 2A-mCherry-2A-GCaMP6m (C2M2G) (B).

(C) Confocal images of the C2M2G hippocampus (female; P5). Anti-NeuN (neurons), anti-GFAP (astrocytes), anti-Iba-1 (microglia), and anti-GFP (GCaMP6m) were used for staining. Note that GCaMP6m expression is confined to microglia. The inserts on the right show the marked area at higher magnification. Scale bars: 10 and 100 μm; n = 3 mice, 10 slices.

(D) Two-photon live-cell recording of hippocampal microglia *in situ*. Left: GCaMP6m fluorescence images under basal conditions and in presence of 1 mM ATP. Right: recordings of microglial  $\text{Ca}^{2+}$  elevations under control conditions (spontaneous activity; red arrows) and upon application of 1 mM ATP. The scaling of the amplitudes refers to an 8-bit range. Scale bar: 20 μm.

(E and F) Percentage of responding cells (E) and average amplitudes (F) during 5-min recordings under basal conditions and upon ATP (1 mM) application from P5–P6 (white bars) and P45–P70 (black bars) mice. Spontaneous  $\text{Ca}^{2+}$  responses decreased age-dependently. We only considered ATP-responding cells for our analysis (ATP: 100%). P5–P6: n = 8 mice, 17 slices, 406 cells; P45–P70: 5 mice, n = 19 slices, 577 cells.

(G) Summary of rise and decay times of spontaneous  $\text{Ca}^{2+}$  elevations.

Data in (E)–(G) are presented as means ± SEM. Statistical significance: n.s., p ≥ 0.05; \*\*p ≤ 0.01.

spontaneous  $\text{Ca}^{2+}$  elevations of microglia from C2G and C2M2G hippocampi (Figure S3).

We next analyzed ATP-evoked increases in GCaMP6m fluorescence, which refer to the activity of microglial purinergic P2X and P2Y receptors (Boucsein et al., 2003; Korvers et al., 2016; Kettenmann et al., 2011). There was, indeed, a robust increase in GCaMP6m fluorescence upon application of 1 mM ATP (Figure 1D), with amplitudes of  $6.1 \pm 0.4$  AU (P5–6) and  $6.4 \pm 0.4$  AU (P45–70) (Figure S3), which were reversible upon wash-out of ATP, indicating that microglial  $\text{Ca}^{2+}$  levels are reliably monitored by the GCaMP6m transgene. We also found reliable ATP-evoked GCaMP6m fluorescence increases in other brain regions (data not shown), and there were no statistical differences between the C2G and C2M2G mouse models (Figure S3). We, therefore, conclude that the two mouse models are valid to be used for monitoring microglial  $\text{Ca}^{2+}$  levels in various brain regions and at different developmental time points.

### Hippocampal microglia in neonatal brain slices respond to neurotransmitter release upon Schaffer collateral stimulation

To investigate whether microglia can sense synaptic activity, we used neonatal C2M2G mice to investigate microglial  $\text{Ca}^{2+}$  level changes in the hippocampal CA1 region during and after electrical stimulation of the Schaffer collateral pathway stimulation (STM). An electrical stimulation pipette was placed at CA3 stratum radiatum of P5–6 hippocampal brain slices to evoke single high-frequency bursts (100 pulses at 100 Hz). In parallel to that stimulation, we monitored microglial mCherry and GCaMP6m fluorescence levels in the CA1 region by live-cell imaging using an upright Zeiss LSM 880 and a 20 $\times$  objective. As shown in Figure 2, high-frequency Schaffer collateral stimulation led to transient  $\text{Ca}^{2+}$  elevations in microglia. Responses were observed only in a subpopulation of cells and occurred in both somata and processes (somata:  $37.6\% \pm 4.1\%$ ,  $n = 14$  mice, 19 slices, 209 cells; processes:  $45.4\% \pm 4.3\%$ ,  $n = 14$  mice, 19 slices, 599 cells;  $p = 0.5961$ ). In 61 of 209 microglia, we could not detect the processes and could, therefore, not determine process  $\text{Ca}^{2+}$  responses. However, there were never process responses after electrical stimulation without responses in the respective soma, suggesting that there was no subcellular confinement of microglial responses upon electrical stimulation. We also quantified spontaneous  $\text{Ca}^{2+}$  elevations (Figure 2E, “basal”) on a subcellular level in microglia. Interestingly, although these events often occurred at different time points in somata and processes of the same cell (Figure S4), the overall response rate was similar within a period of 2 min (somata:  $10.4\% \pm 4.2\%$ ; processes:  $10.4\% \pm 4.4\%$ ;  $n = 13$  mice, 18 slices, 208 cells;  $p = 0.9666$ ; Figure 2E). ATP (1 mM) application at the end of each experiment led to  $\text{Ca}^{2+}$  increases in 100% of the somata and  $95.02\% \pm 1.6\%$  of the observed processes ( $n = 14$  mice, 19 slices, 209 cells;  $p = 0.9102$ ; Figures 2D and 2E). Taken together, these data demonstrate that a subpopulation of microglia in the hippocampal CA1 region respond to electrical stimulation of the Schaffer collateral pathway with  $\text{Ca}^{2+}$  elevations in their somata and processes.

We next aimed to characterize the spatial and temporal properties of microglia responses upon Schaffer collateral stimulation

and monitored microglial  $\text{Ca}^{2+}$  levels by two-photon live cell imaging using a 10 $\times$  objective to obtain more global recordings from the CA3–CA1 region of the hippocampus (Figure 3A). We focused on somatic responses because there was no evidence for profound differences in the subcellular distribution of STM-evoked  $\text{Ca}^{2+}$  elevations (see above). An electrical stimulation pipette was placed at CA3 stratum radiatum of a P5/6 hippocampal brain slice from C2G or C2M2G mice to evoke high-frequency bursts (a single train of 100 pulses at 100 Hz). Another pipette was placed in the CA1 region to record the resulting field potential responses, which had an average amplitude of  $3.0 \pm 0.6$  mV at the first field excitatory postsynaptic potential (fEPSP) peak of the stimulation train ( $n = 25$  mice, 35 slices). The distance between the two pipettes was around 500  $\mu\text{m}$ . Also in this experimental setting, a subpopulation of microglia responded to STM;  $66.9\% \pm 3.6\%$  of ATP-responding microglia between the stimulation and recording pipettes responded to Schaffer collateral stimulation ( $n = 25$  mice, 35 slices, 1174 cells) within the first 60 s after the stimulus (STM). The majority ( $91.4\% \pm 1.6\%$ ) of the STM-responding microglia responded also to ATP. Microglial  $\text{Ca}^{2+}$  responses upon neuronal stimulation lasted much longer than the stimulation itself and were transient with a fast initial rise and a slow exponential decay. We analyzed the spatial and temporal occurrence of STM-mediated microglial  $\text{Ca}^{2+}$  responses in neonatal hippocampi. As shown in Figure 3C, most events started within the first 10 s after stimulation, and the cells being located closer to the stimulus pipette responded earlier than the more distant cells, indicating a wave-like propagation of microglial responses with an average speed of  $41.7 \pm 1.4$   $\mu\text{m}/\text{s}$ , starting from the electrical stimulus. To look specifically at potential microglial responses upon synaptic transmission, we constrained our analysis to microglia that were located more distant from the stimulus pipette ( $>300$   $\mu\text{m}$ ), thus, mainly in the receiving region CA1. Furthermore, to separate those responses that potentially occur because of synaptic release of neurotransmitters, we considered only responses within the first 10 s after the stimulation train (see gray dashed boxes in Figure 3C). In neonatal hippocampi,  $29.6\% \pm 5.2\%$  ( $n = 21$  mice, 24 slices, 297 cells; Figure 3D) of these microglia responded to high-frequency stimulation. We next tested whether and how microglia respond upon weaker stimulation paradigms and decreased the number of pulses. As shown in Figure 3E, a similarly high population of microglia responded to a single train of either 10, 20, or 100 pulses at 100 Hz, whereas there were only little responses upon a single pulse or five pulses, indicating an activity-dependent mechanism. We next tested whether microglial responses upon electrical stimulation rely on neuronal activity and blocked the generation of action potentials by tetrodotoxin (TTX; 1  $\mu\text{M}$ ; Figures 3C and 3D), which expectedly led to a complete loss of fEPSPs (Figure 3C, TTX, inset). The response rate of microglia in the presence of TTX ( $3.7\% \pm 1.5\%$ ;  $n = 15$  mice, 25 slices, 545 cells) was significantly reduced in comparison with control conditions ( $p < 0.0001$ ) and not significantly different from spontaneous activity in the presence of TTX ( $3.1\% \pm 0.7\%$ ;  $p = 0.6578$ ; Figure 3D). We next inhibited neuronal transmission by the blockade of postsynaptic receptors to more specifically elucidate the effect of neurotransmitter release on microglial  $\text{Ca}^{2+}$  responses. We used a combination of 6-cyano-

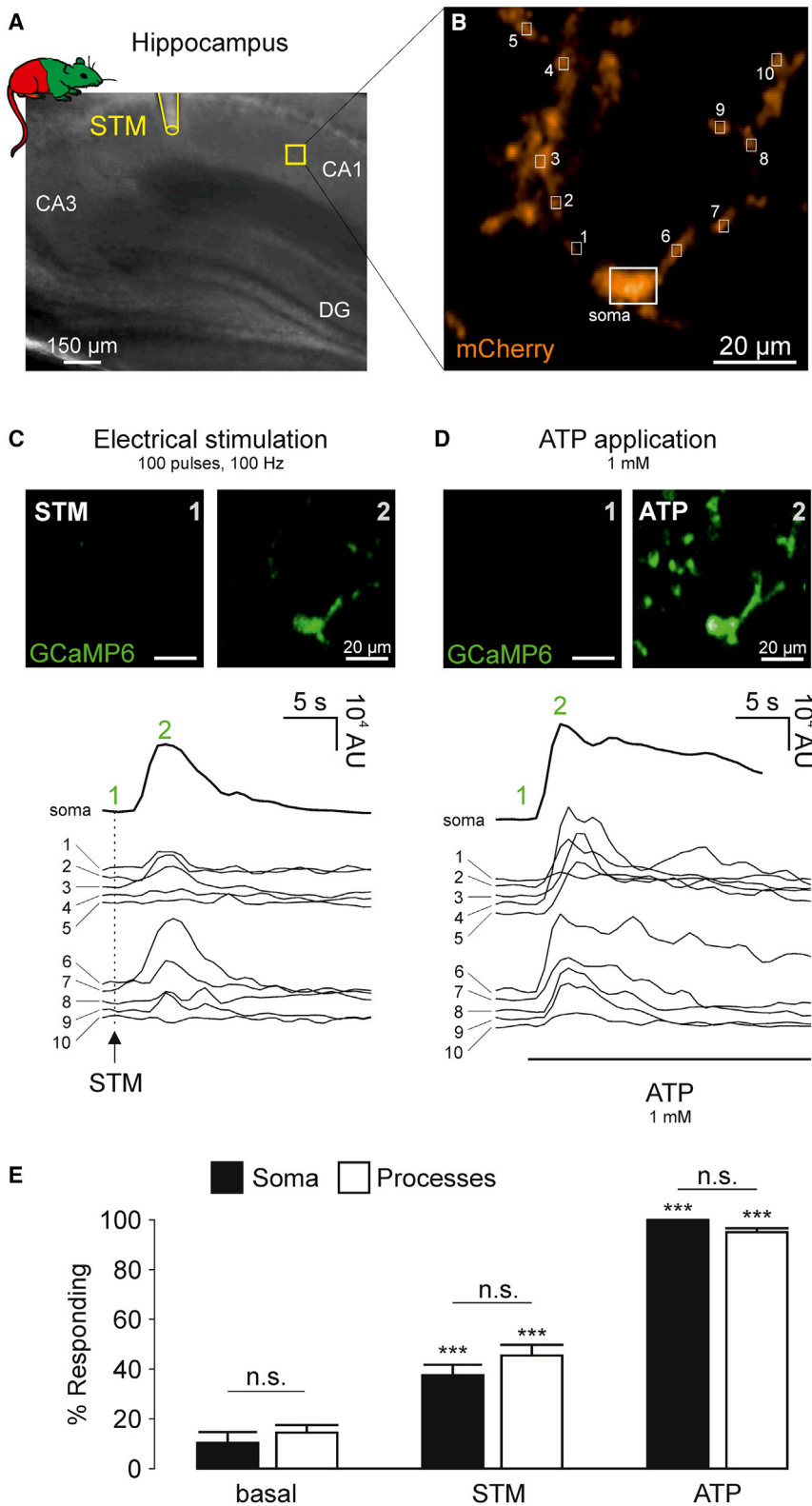


**Figure 2. Microglia in the CA1 region respond to Schaffer collateral stimulation**

(A) Transmission light image of a P5 C2M2G hippocampus. DG, dentate gyrus; CA1/3, cornus ammonis region 1/3. Stimulation pipette and recording field—see (B), (C), and (D)—are indicated in yellow. Scale bar: 150  $\mu$ m.

(B) Confocal image of a responding microglia during live-cell recording visualized by its fluorescence of transgenic mCherry. Regions of interest (soma and process regions 1–10) of traces shown in (C) and (D) are indicated. Scale bar: 20  $\mu$ m.

(C) Top, GCaMP6m fluorescence of microglia shown in (B), before a single train of 100 pulses at 100 Hz (0 s) and at the peak of the somatic response. A baseline image (mean intensity projection from 6 to 1 s before the stimulus) was subtracted to highlight the  $\text{Ca}^{2+}$  response. Scale bar: 20  $\mu$ m. Bottom,  $\text{Ca}^{2+}$  traces of regions of interest (ROIs) indicated in (B), during and after stimulation. Scaling of the amplitudes refers to a 16-bit range. Scale bar: 20  $\mu$ m.

(D) Same as (C) but during the application of ATP (1 mM).

(E) Quantification of microglial somatic and process  $\text{Ca}^{2+}$  elevations in hippocampal CA1 at P5 occurring spontaneously (“basal”), after electrical stimulation (“STM”), and during ATP application. There was no significant difference in subcellular response rates. Significance statements above the bars are comparisons to the respective spontaneous responses (“basal”).  $n = 14$  mice, 19 slices, 209 cells. Data are presented as means  $\pm$  SEM. Statistical significance: n.s.,  $p \geq 0.05$ ; \*\*\* $p \leq 0.001$ .

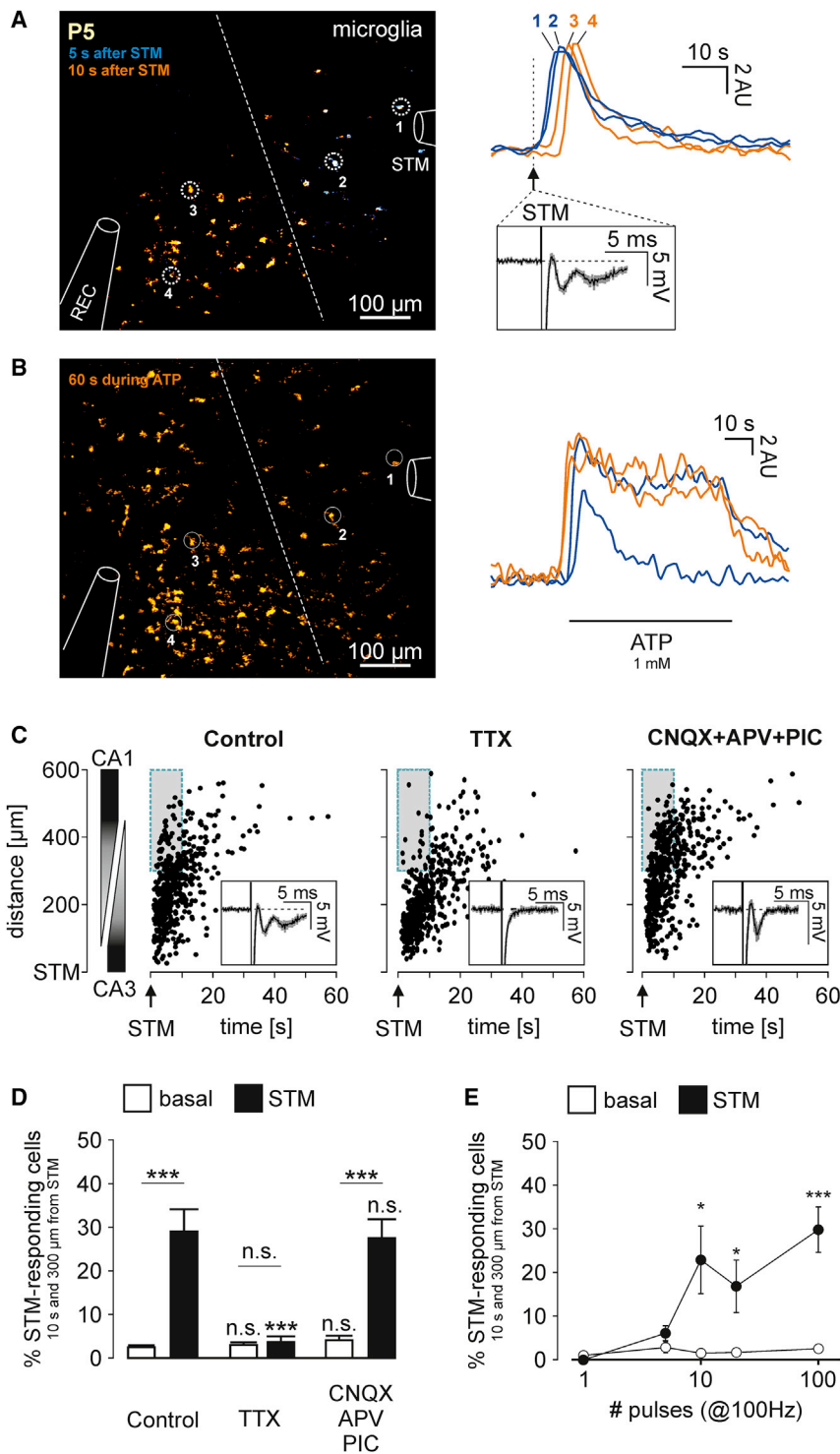


**Figure 3. Microglia responses to Schaffer collateral stimulation depend on action potentials**

(A) Left: two-photon image of responding microglia after Schaffer collateral stimulation. A stimulation pipette (STM) was placed in CA3 stratum radiatum (P5) and a recording pipette (REC) in the CA1. In blue, the mean intensity projection from images taken 0–5 s after stimulation and in orange, 5–10 s after stimulation (100 pulses at 100 Hz). A baseline image (as explained in Figure 2C) was subtracted to highlight responding cells. The white dotted line indicates 300- $\mu$ m distance from the STM pipette. Only microglia left from this line were considered for the analysis in (D). Right: stimulation-evoked microglial  $\text{Ca}^{2+}$  responses. The scaling of the amplitudes refers to an 8-bit range. Inset: field potential responses to STM. Scale bar: 100  $\mu$ m.

(B) Microglia as described in (A) but during ATP application.

(C) Spatiotemporal distribution of microglial  $\text{Ca}^{2+}$  responses after stimulation under control conditions (left) and in presence of TTX (1  $\mu$ M; middle) or CNQX+APV+PIC (right). Each dot represents one stimulation-responding cell. Distance from STM pipette was obtained in the two-dimensional (2D) representation. See (A). Gray dashed boxes indicate cells located at least 300  $\mu$ m from the STM and with responses within the first 10 s after stimulation. Insets: averaged field potential responses upon the first stimulus train pulse.

(D) Quantification of microglia responding to the stimulation under control conditions, TTX (1  $\mu$ M), or CNQX (10  $\mu$ M) + APV (50  $\mu$ M) + picrotoxin (PIC; 10  $\mu$ M). Only responses in the dashed boxes in (C) were analyzed. All conditions are compared with the spontaneous responses quantified in the minute before stimulation (“basal”). Data are presented as means  $\pm$  SEM. Statistical significance: n.s.,  $p \geq 0.05$ ; \*\*\* $p \leq 0.001$ . Control:  $n = 21$  mice, 24 slices, 297 cells; TTX:  $n = 15$  mice, 25 slices, 545 cells; CNQX+APV+PIC:  $n = 13$  mice, 20 slices, 333 cells.

(E) Microglial response rates upon Schaffer collateral stimulation with different number of pulses.  $n = 20$  mice, 28 slices, 1090 cells.

7-nitroquinoxaline-2,3-dione (CNQX; 10  $\mu$ M), 2-amino-5-phosphonopentanoic acid (APV; 50  $\mu$ M), and picrotoxin (PIC; 10  $\mu$ M) to inhibit ionotropic glycine, GABA and glutamate receptors that are putatively located on the postsynaptic side of CA3-CA1 synapses. Electrical stimulation in CA3 should,

therefore, still lead to the release of neurotransmitters from presynapses under these conditions. The combined treatment (CNQX+APV+PIC) did block the fEPSP, as expected, but not the fiber volley component of the field potential responses upon electrical stimulation (Figure 3C, inset). Notably, microglial responses upon electrical stimulation persisted under these conditions, with a total of  $28.2\% \pm 4.4\%$  STM-responding microglia ( $n = 13$  mice, 20 slices, 333 cells), which was not significantly different from responses under control conditions ( $p = 0.8316$ ). These data support the notion that the microglial  $\text{Ca}^{2+}$  waves are not dependent on postsynaptic responses but potentially on neurotransmitter release from presynaptic sites.

### Hippocampal microglia express functional GABA<sub>B</sub> receptors and respond to external glutamate and GABA

Microglia were previously shown to express functional neurotransmitter receptors, including metabotropic GABA and glutamate receptors (GABA<sub>B</sub> and mGluR, respectively; Kuhn et al., 2004; Pocock and Kettenmann, 2007) and could, therefore, directly sense neurotransmitters that spill over at CA3–CA1 synapses upon Schaffer collateral stimulation. To test for microglial neurotransmitter receptors *in situ*, we revisited the recent findings and investigated whether neonatal (P5/6) hippocampal microglia are responsive to the external application of GABA and glutamate. Indeed, as shown in Figures 4A and 4B, a substantial population of microglia responded to the application of GABA (51.8% ± 6.0%; 100 μM; n = 11 mice, 28 slices, 448 cells). Responses could be mimicked by the GABA<sub>B</sub> receptor agonist baclofen (500 μM; 62.0 ± 6.6%; n = 5 mice, 12 slices, 168 cells; p = 0.2429 versus GABA) and were significantly reduced by the selective GABA<sub>B</sub>R inhibitor CGP55845 (1 μM; 9.2% ± 1.1%; n = 4 mice, 11 slices, 247 cells; p < 0.001 compared with GABA). Furthermore, the application of the selective ionotropic GABA<sub>A</sub> receptor agonist muscimol (100 μM) evoked responses in only 13.8% ± 3.4% of the microglia (n = 6 mice, 12 slices, 584 cells; p < 0.001 versus GABA; p = 0.6714 versus basal), and the inhibition of ionotropic neurotransmitter receptors by using CNQX+APV+PIC (53.1% ± 12.4%; n = 3 mice, 5 slices, 233 cells; Figure 4B) had no significant effect on GABA-mediated Ca<sup>2+</sup> elevations in microglia. Taken together, these data suggest that microglia respond to GABA via intrinsic GABA<sub>B</sub> receptors, a notion that is further supported by published transcriptomics datasets (for a meta-analysis, see Figure S5). We additionally performed immunohistochemical stainings and found, in accordance with our functional data and with a recent study on cortical microglia (Favuzzi et al., 2021), *Gabbr1* expression in around 61.5% ± 36.1%/65.9% of the *Iba1*<sup>+</sup> cells in P5 hippocampal slices (n = 163 cells/14 slices; Figure 4C). Although our data indicate a high emergence of microglia expressing functional GABA<sub>B</sub> receptors, we found no difference in the appearance of spontaneous Ca<sup>2+</sup> elevations when these receptors were blocked (Figure S8).

The application of external glutamate (100 μM) led also to Ca<sup>2+</sup> responses in a significant portion of hippocampal microglia (50.5% ± 5.9%; 100 μM; n = 12 mice, 25 slices, 831 cells; Figures 4D and 4E). Microglia express—although on a very low level—group II metabotropic glutamate receptors (mGluR II; Figure S5; Tabula Muris Consortium, 2018). However, the external application of the specific mGluR II agonist LY379268 (100 nM) did not evoke appreciable Ca<sup>2+</sup> responses (1.6% ± 1.6%; n = 5 mice, 10 slices, 92 cells). Likewise, the blockade of mGluR II by LY341495 (1 μM)—either alone (49.4% ± 20.2%, n = 5 mice, 5 slices, 79 cells; p = 0.9626 versus glutamate alone; data not shown) or in combination with the mGluR I and III inhibitors DL-AP3 (500 μM) and CPPG (10 μM; 63.1% ± 10.3%, n = 4 mice, 12 slices, 293 cells; p = 0.1010; Figure 4E)—did not affect glutamate-induced Ca<sup>2+</sup> elevations, thus, ruling out the involvement of metabotropic glutamate receptors in microglial responses to glutamate. Glutamate can also trigger neuronal ATP release (Eyo et al., 2014) and could theoretically increase microglial Ca<sup>2+</sup> via puri-

nergic signaling. However, the presence of 1 μM AR-C69931 did not affect microglia response rates to glutamate (Figure S7), ruling out microglial *P2ry12* as potential signal transducer. Surprisingly, the blockade of ionotropic glutamate receptors with a combination of CNQX+APV+PIC also had no effect on microglial responses to glutamate. Accordingly, the combined application of the ionotropic glutamate receptor agonists NMDA (100 μM) and kainate (100 μM) evoked responses in only 7.2% ± 1.9% of microglia (n = 4 mice, 12 slices, 499 cells), which was similar to spontaneous activity (p = 0.3597). We, therefore, conclude that metabotropic and ionotropic glutamate receptors are not involved in microglial responses upon external glutamate, suggesting an alternative signaling pathway that might include neurons or astrocytes as the potential source for secondary messenger molecules that stimulate microglial Ca<sup>2+</sup> responses upon glutamate application.

In an attempt to further elucidate the mechanism of microglia glutamate responses, we considered glutamate transporters (EAAT), which can evoke a net influx of Na<sup>+</sup> and Cl<sup>-</sup> upon extracellular glutamate uptake. D-aspartate (D-Asp; 100 μM) is a transportable substrate of EAAT and led, indeed, to microglial Ca<sup>2+</sup> increases in 42.9% ± 5.9% of hippocampal microglia (n = 7 mice, 14 slices, 361 cells; Figure 4E), which was similar to microglial responses rates to glutamate (p = 0.5431). EAATs are primarily expressed in neurons and astrocytes in a cell-type-specific fashion, with EAAT1/2 (*Slc1a3/2*) present in astrocytes and EAAT4 (*Slc1a6*) present in neurons (Rose et al., 2018; Zhang et al., 2014) (Figure S5). The subtype-specific inhibition of EAAT1/2 transporters by (2S,3S)-3-[3-[4-(trifluoromethyl)benzoylamino]benzyloxy]aspartate (TFB-TBOA) (200 nM) completely blocked microglial responses to glutamate and D-Asp (Figure 4E), indicating the involvement of astrocytic glutamate transport and suggesting a subsequent release of messenger molecules from astrocytes toward microglia. It was previously demonstrated by Héja et al. (2012) that, in the rodent neonatal hippocampus, astrocytic glutamate transporters are co-localized with GAT3 GABA transporters and that astrocytic glutamate uptake is a prerequisite for the non-synaptic release of GABA from astrocytes (Wu et al., 2007). As microglia responded *in situ* to GABA via GABA<sub>B</sub> receptors (see above), astrocytic GABA release upon glutamate uptake could, indeed, trigger microglial glutamate responses. To test for that possibility, we used CGP55845 (1 μM) to inhibit microglial GABA<sub>B</sub> receptors and determined microglial responses upon glutamate. Strikingly, microglial responses upon glutamate were completely blocked by GABA<sub>B</sub>R inhibition (4.2% ± 1.4%; n = 4 mice, 7 slices, 325 cells; p = 0.0015 versus glutamate alone Figure 4E). We, therefore, conclude that GABA<sub>B</sub> receptors on hippocampal microglia can indirectly sense elevations in extracellular glutamate via astrocytic ion transporter-mediated GABA release.

### Microglial Ca<sup>2+</sup> responses to STM are mediated by glutamate uptake-coupled release of GABA from astrocytes

We next tested whether microglial responses to Schaffer collateral stimulation depend on GABA<sub>B</sub> receptor activity and whether ion transporters are involved. We used a similar setting as in Figure 3 and performed two-photon live cell imaging using a 10× objective to monitor somatic Ca<sup>2+</sup> elevations in a larger population

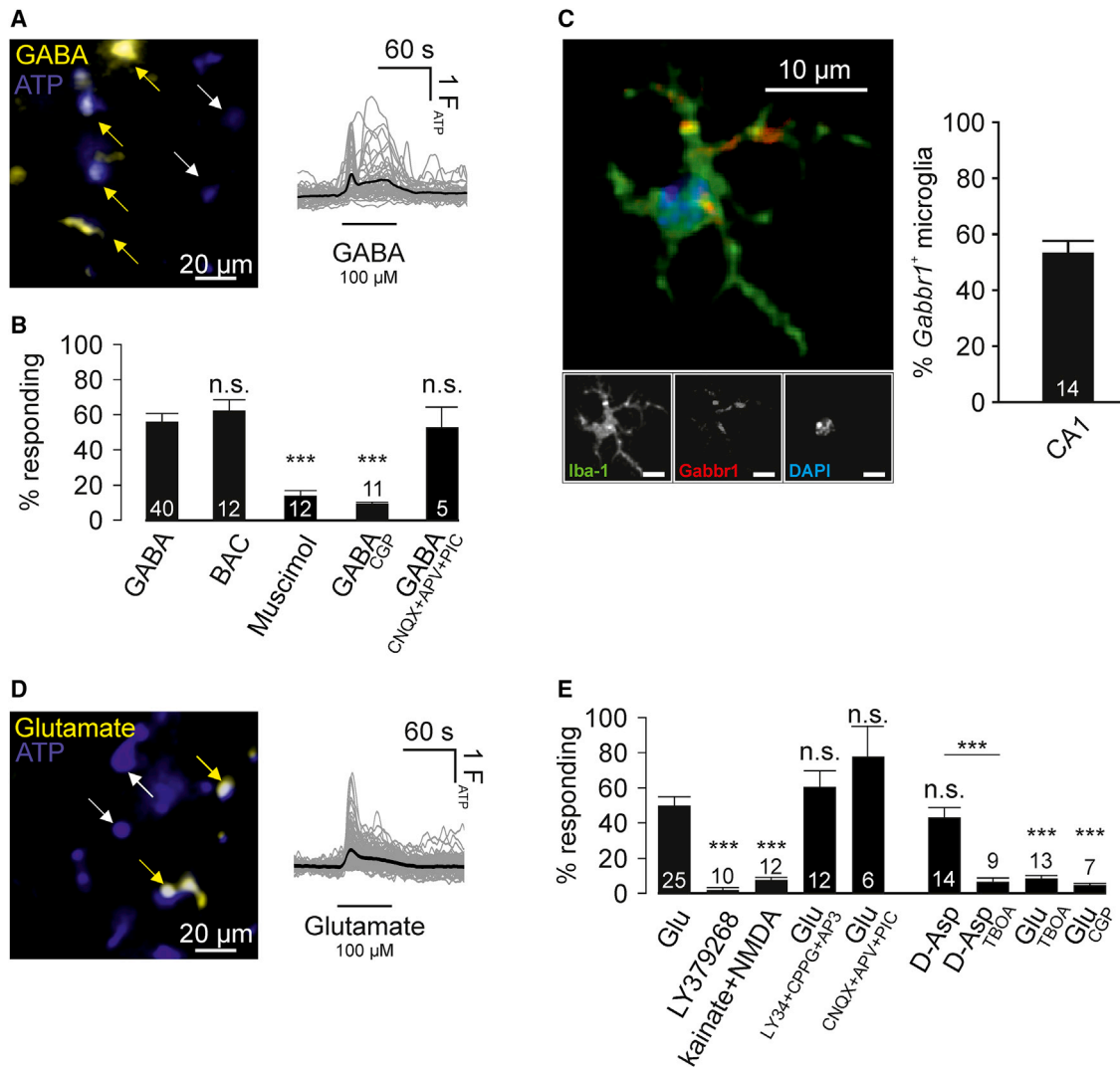


**Figure 4. Microglia respond to GABA and glutamate via GABA<sub>B</sub> receptors**

(A) Left: representative microglial cells during live cell recordings from neonatal hippocampal brain slices during GABA (yellow mask) and ATP (blue mask) application. Images were generated by subtraction of the video frames before application from frames in the presence of the given substances. GABA-responding microglia are indicated with a yellow arrow; non-responding with a white arrow. Right: microglial Ca<sup>2+</sup> traces of responding cells from all experiments before, during, and after external GABA application (100 μM; top) are shown in gray. Black traces are the average of all gray traces. Amplitudes were normalized to the peak of the ATP response amplitude (=1 F<sub>ATP</sub>). Scale bar: 20 μm.

(B) Percentage of microglia responding to GABA (100 μM; n = 11 mice, 28 slices, 448 cells), the GABA<sub>B</sub>R agonist Baclofen (500 μM; n = 5 mice, 12 slices, 168 cells) and the combination of GABA (100 μM) and the GABA<sub>B</sub>R antagonist CGP55845 (1 μM; n = 4 mice, 11 slices, 247 cells) as well as the GABAAR agonist Muscimol (100 μM; n = 6 mice, 12 slices, 584 cells) and GABA together with an ionotropic receptor blocker cocktail (10 μM CNQX + 50 μM APV + 10 μM picrotoxin; n = 3 mice, 5 slices, 233 cells). Significance statements above the bars indicate comparisons against GABA response rate.

(C) Left: confocal image of a P5 microglial cell from the CA1 region stained for *Iba1* (green) and *Gabbr1* (red). DAPI channel is shown in blue. Right: quantification of immunohistochemical stainings reveals *Gabbr1* expression in a subpopulation of *Iba1*<sup>+</sup> cells. Number on the bar indicates the number of analyzed slices. Scale bar: 10 μm. n = 163 cells/14 slices.

(D) Representative image (left) and Ca<sup>2+</sup> traces (right) of responding cells as described in (A), but in the presence of glutamate (100 μM; yellow mask) and ATP (blue mask). Scale bar: 20 μm.

(E) Percentage of microglia responding to Glu (100 μM; n = 12 mice, 25 slices, 831 cells), mGluR group II agonist LY379268 (100 nM; n = 5 mice, 5 slices, 79 cells) and the combination of Glu (100 μM) and the mGluR groups I, II, and III antagonists DL-AP3 (500 μM), LY341495 (1 μM), and CPPG (10 μM), respectively (n = 4 mice, 12 slices, 293 cells). Furthermore, responses to the ionotropic glutamate receptor agonists NMDA (100 μM) and kainate (100 μM; n = 4 mice, 12 slices, 499 cells) and the sensitivity of Glu responses to blockade of ionotropic receptors (10 μM CNQX + 50 μM APV + 10 μM picrotoxin; n = 3 mice, 6 slices, 269 cells) were investigated. Also shown is the percentage of microglia responding to D-Asp (100 μM; n = 7 mice, 14 slices, 361 cells) and sensitivity of these responses to the EAAT1/2 inhibitor TFB-TBOA (200 nM; n = 9 mice, 13 slices, 469 cells). Furthermore, the impact of the GABA<sub>B</sub>R antagonist CGP55845 (1 μM; n = 4 mice, 7 slices, 325 cells) on Glu responses was tested. All significance statements above the bars indicate comparisons against glutamate response rates.

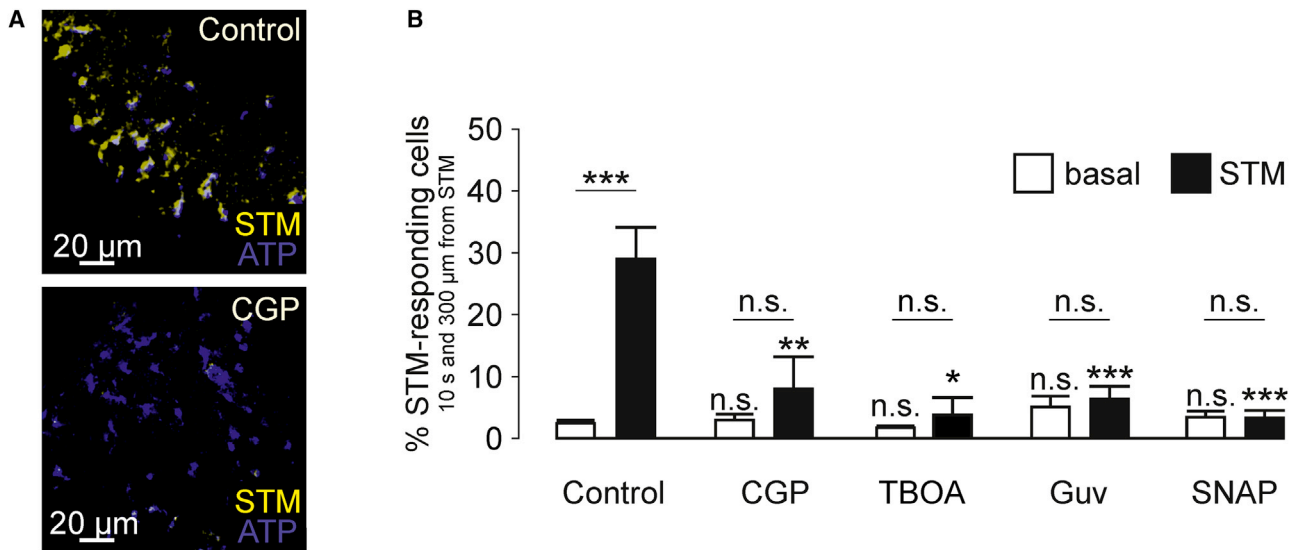


**Figure 5. Microglial  $\text{Ca}^{2+}$  responses to STM depend on astrocytic transporters and  $\text{GABA}_B\text{R}$**

(A) Overlay of P5 microglia  $\text{Ca}^{2+}$  responses to ATP (1 mM; blue mask) and STM (yellow mask) under control conditions (top) and in the presence of the  $\text{GABA}_B\text{R}$  blocker CGP55845 (1  $\mu\text{M}$ ). Note that the two overlay images are from two different experiments. Scale bar: 20  $\mu\text{m}$ .

(B) Quantification of STM-responding microglia under control conditions and during application of CGP55845 (1  $\mu\text{M}$ ; n = 9 mice, 18 slices, 323 cells), the selective glutamate transporter EAAT1-2 blocker TFB-TBOA (200 nM; n = 8 mice, 17 slices, 1,053 cells), the GABA uptake inhibitor Guvacine (300  $\mu\text{M}$ ; n = 8 mice, 12 slices, 223 cells) or the GAT3-specific blocker SNAP5114 (40  $\mu\text{M}$ ; n = 8 mice, 12 slices, 439 cells).

of CA3/CA1 microglia. An electrical stimulation pipette placed at CA3 stratum radiatum was used to evoke high-frequency bursts (100 pulses at 100 Hz). Strikingly, in the presence of CGP55845 (1  $\mu\text{M}$ ), only  $8.3\% \pm 5.2\%$  of the microglia responded to high-frequency stimulation (n = 9 mice, 18 slices, 323 cells), which was similar to basal activity ( $3.0\% \pm 1.0\%$ ;  $p = 0.3350$ ) and significantly less than stimulation-evoked responses under control conditions ( $p = 0.0062$ ; Figures 5A and 5B), indicating the involvement of  $\text{GABA}_B$  receptors. We furthermore blocked astrocytic glutamate transporters and found that the application of TFB-TBOA (200 nM) led also to a significant reduction of microglial  $\text{Ca}^{2+}$  responses to STM, indicating the involvement of astrocytic glutamate transporters in microglial  $\text{Ca}^{2+}$  responses to STM ( $5.4\% \pm 2.1\%$  of the responses; n = 8 mice, 17 slices, 1,053 cells;  $p < 0.001$  versus control STM; Figure 5B). We finally tested the blockade of GABA transporters. Guvacine (300  $\mu\text{M}$ ) acts on neuronal (GAT1) and astrocytic (GAT3) GABA transporters and blocked microglial responses to electrical stimulation to  $6.5\% \pm 2.1\%$  (n = 8 mice, 12 slices, 223 cells; Figure 5B), which was significantly less than under control conditions ( $p < 0.001$ ). Furthermore, SNAP5114 (40  $\mu\text{M}$ ), which selectively inhibits GAT3 transporters on astrocytes, also completely blocked microglial responses upon STM ( $3.4\% \pm 1.3\%$ ; n = 8 mice, 12 slices, 439 cells;  $p < 0.0001$  versus control STM). Of note, the CA1 field-potential responses were not reduced by the application of CGP55845, TFB-TBOA, guvacine, or SNAP5114 (Figure S9), indicating that we apparently did not inhibit synaptic release of neurotransmitters in these experiments. Taken together, these data suggest that neuronal stimulation in the neonatal hippocampus is sensed by microglia through a conversion of glutamate to GABA signals by astrocytic amino acid transporters.

We studied astrocytes and their  $\text{Ca}^{2+}$  level changes upon stimulation of the Schaffer Collateral pathway (Schipke et al., 2002; Shigetomi et al., 2018) to estimate their response behavior in the presence and absence of different blockers (Figures 6A–6C). Neonatal (P5–P6) hippocampal brain slices from C57/Bl6 mice were loaded with the  $\text{Ca}^{2+}$  indicator Fluo4-AM which is taken up predominantly by astrocytes (Schipke et al., 2002). Electrical stimulation in CA3 led indeed to  $\text{Ca}^{2+}$  responses in most astrocytes between the two stimulation pipettes. The constrained analysis of astrocytes that were located at a distance of at least 300  $\mu\text{m}$  from the stimulation pipette and of responses that occurred within 10 s after the stimulation resulted in a response rate of  $57.4\% \pm 9.2\%$  astrocytes responding to STM (n = 5 mice, 12 slices, 641 cells). Interestingly, when comparing the time courses of microglial and astrocytic responses upon Schaffer collateral stimulation, astrocytic responses clearly preceded microglial responses on average by 3.4 s (Figure 6D), suggesting that astrocytes are indeed primary receivers of synaptic signals. In the presence of TTX, astrocytic responses were significantly decreased to  $13.9\% \pm 5.1\%$  (n = 5 mice, 12 slices, 293 cells;  $p < 0.001$ ; Figure 6C), indicating their dependence on neuronal action potentials. Applying a combination of CNQX (10  $\mu\text{M}$ ), APV (50  $\mu\text{M}$ ) and picrotoxin (PIC; 10  $\mu\text{M}$ ) to block postsynaptic ionotropic GABA and glutamate receptors did not, however, reduce the percentage of STM-responding astrocytes, indicating the importance of presynaptic release ( $60.4\% \pm 8.6\%$ ; n = 8 mice, 10 slices, 200 cells;  $p = 0.8118$  compared with the control). The propagation of astrocytic  $\text{Ca}^{2+}$  waves was not affected by the  $\text{GABA}_B\text{R}$  inhibitor CGP55845 ( $57.7\% \pm 10.4\%$ ; n = 3 mice, 6 slices, 284 cells;  $p = 0.9065$ ; Figure 6C) but by the blockade of

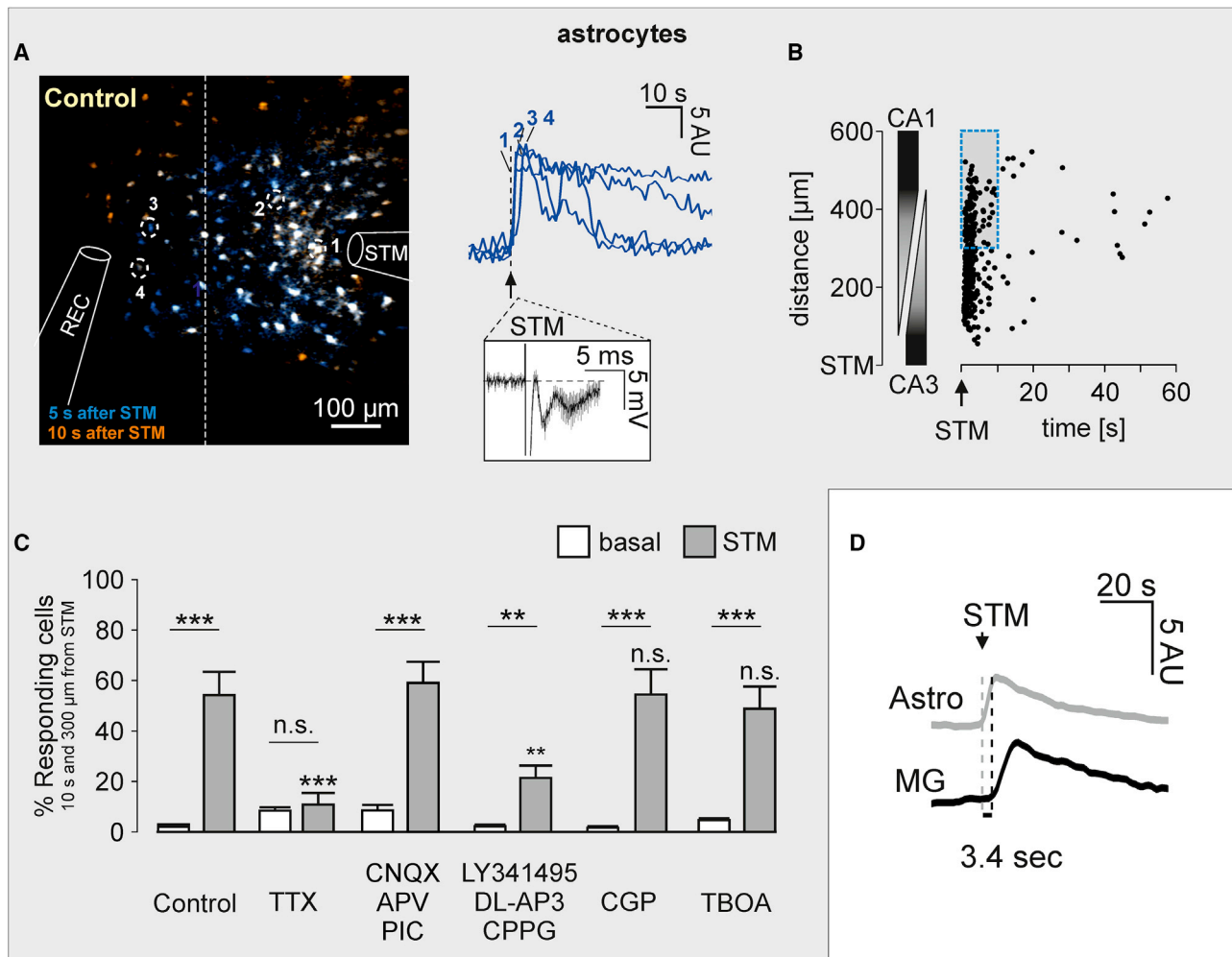


**Figure 6. Astrocytic  $\text{Ca}^{2+}$  responses to electrical stimulation depend on action potentials**

(A) Left: image from a representative 2-photon astrocytic  $\text{Ca}^{2+}$  recording after Schaffer collateral stimulation (as described in Figure 3A for microglia). Slices were loaded with 10  $\mu\text{M}$  Fluo4-AM to visualize astrocytic  $\text{Ca}^{2+}$  level changes. Right: stimulation-evoked astrocytic  $\text{Ca}^{2+}$  responses of the ROIs indicated on the left. Scaling of amplitudes refers to an 8-bit range. Inset: averaged field potential responses upon the first stimulus train pulse. Scale bar: 100  $\mu\text{m}$ .

(B) Spatiotemporal distribution of astrocyte  $\text{Ca}^{2+}$  responses after electrical stimulation under control conditions, as used for microglia (details in Figure 3C).

(C) Quantification of STM-responding astrocytes from P5–P6 mice under control conditions ( $n = 5$  mice; 12 slices, 641 cells) and in the presence of TTX ( $n = 5$  mice, 12 slices, 293 cells), CNQX (10  $\mu\text{M}$ ) + APV (50  $\mu\text{M}$ ) + PIC (10  $\mu\text{M}$ ;  $n = 8$  mice, 10 slices, 200 cells), the GABA<sub>B</sub> inhibitor CGP55845 (1  $\mu\text{M}$ ;  $n = 3$  mice, 6 slices, 284 cells), the mGluR groups I, II, and III antagonists DL-AP3 (500  $\mu\text{M}$ ), LY341495 (1  $\mu\text{M}$ ) and CPPG (10  $\mu\text{M}$ ;  $n = 7$  mice, 12 slices, 394 cells), or the selective glutamate transporter EAAT1-2 blocker TFB-TBOA (200 nM;  $n = 4$  mice, 8 slices, 408 cells). To estimate the portion of spontaneous responses, we also quantified  $\text{Ca}^{2+}$  responses 10 s before stimulation (“basal”). Data are presented as means  $\pm$  SEM. Statistical significance is indicated as followed: n.s.,  $p \geq 0.05$ ; \* $p \leq 0.05$ , \*\* $p \leq 0.01$ , \*\*\* $p \leq 0.001$ .

(D) Merged time courses of microglial and astrocytic  $\text{Ca}^{2+}$  elevations upon electrical stimulation indicates that the astrocytic responses precede the microglial ones by on average 3.4 s.

metabotropic glutamate receptors ( $21.4\% \pm 4.9\%$ ;  $n = 7$  mice, 12 slices, 394 cells;  $p = 0.0040$ ). TFB-TBOA itself had an effect on astrocytic  $\text{Ca}^{2+}$  levels (Figure S6) but did not significantly affect the astrocytic  $\text{Ca}^{2+}$  responses to neuronal stimulation ( $50.1\% \pm 9.0\%$ ;  $n = 4$  mice, 8 slices, 408 cells;  $p = 0.7845$  versus the control STM).

Taken together, these data demonstrate that, in the neonatal hippocampus, Schaffer collateral stimulation is quickly sensed by astrocytes. Microglial responses are few seconds delayed and require (1) the activity of glutamate and GABA transporters,

which are expressed by astrocytes; and (2) GABA<sub>B</sub> receptors, which are intrinsically expressed.

### The stimulation-induced microglial $\text{Ca}^{2+}$ activity is confined to early developmental stages

Because we had demonstrated that microglial responses upon electrical stimulation rely on GABA<sub>B</sub> receptors in neonatal age, we finally asked whether that neuron-microglia communication were also present at adult stages. We, therefore, generated hippocampal brain slices from adult (P49–P70) C2G and C2M2G mice

and applied high-frequency bursts in the CA3 region and monitored microglial  $\text{Ca}^{2+}$  level changes (Figure 7). Intriguingly, in strong contrast to neonatal brain slices, microglia from adult hippocampi only responded sparsely to Schaffer collateral stimulation, although fEPSP amplitudes were even higher than at neonatal ages ( $7.7 \pm 1.5$  mV;  $n = 5$  mice, 18 slices; Figure 7A);  $22.1\% \pm 3.9\%$  of the microglia ( $n = 5$  mice, 18 slices, 573 cells) responded within the first 60 s after stimulation, which was significantly less than at neonatal ages ( $p < 0.001$ ). Notably, responses were located almost completely around the stimulation pipette and did not propagate in a wave-like fashion. Microglia at a greater distance from the stimulation pipette (300  $\mu\text{m}$ ) did not respond ( $n = 4$  mice, 7 slices, 55 cells) during the first 10 s after stimulation. We also tested slices taken from juvenile mice (P13–P15) and found similar results as those in adult ( $14.2\% \pm 4.4\%$ ;  $n = 3$  mice, 9 slices, 110 cells;  $p = 0.1989$  versus spontaneous; Figure 7B), suggesting that microglial  $\text{Ca}^{2+}$  responses in CA1 upon Schaffer collateral stimulation occur only in a developmentally confined period. These data suggest that microglial responses upon electrical stimulation in the neonatal hippocampus require microglial  $\text{GABA}_B$  receptors and GABA release by the astrocytic transporter *GAT3*. We immunostained the neonatal and adult hippocampi for *Iba1* and *Gabbr1* and found no developmental differences in the microglial expression of  $\text{GABA}_B$  receptors (Figure 7C). Furthermore, microglial responses, upon application of 500  $\mu\text{M}$  baclofen, were identical at P5 and P60, indicating that  $\text{GABA}_B$  receptor expression does not explain the lack in microglial responses to electrical stimulation (Figure 7D). Another possible cause could be the operation of the astrocytic GABA transporter *GAT3*, which co-transporters  $2\text{Na}^+$ ,  $1\text{Cl}^-$  and 1GABA (Richerson and Wu, 2003). To potentially stimulate microglial  $\text{GABA}_B$  receptors, *GAT3* necessarily has to operate in the release mode, which could be prevented in adult hippocampal astrocytes by a drop in the internal GABA concentration. We quantified immunohistochemical stainings for GABA and *Gfap* in P5 and P60 hippocampi and found that GABA levels are, indeed, higher in neonatal astrocytes than they are in adult (Figure 7E), indicating developmental changes in astrocytic physiology, which might explain for the different response behavior of microglial cells to neuronal stimulation in neonatal and adult hippocampi.

## DISCUSSION

In the present study, we describe a pathway by which microglia sense neuronal synaptic activity in the hippocampus. This signaling pathway involves the activity of astrocytic GABA and glutamate transporters and microglial  $\text{GABA}_B$  receptors. The identity and location of glutamate and GABA transporters were demonstrated by the use of TFB-TBOA, which specifically blocks EAAT1/2 transporters on astrocytes but not on the neuronal EAAT3 (Tsukada et al., 2005; Shigeri et al., 2004; Divito and Underhill, 2014). Similarly, SNAP5114 selectively inhibits *GAT3*, which is expressed on astrocytes but not neurons (Borden, 1996). It is well established that glutamate released from presynaptic terminals is taken up by astrocytes because of the activity of the glutamate transporter EAAT1/2 (Rose et al., 2018). These transporters use a  $\text{Na}^+$  gradient as energy source for the transport resulting in an increase in intracellular  $\text{Na}^+$  upon glutamate uptake (Rose et al., 2018). GABA

transporters are also linked to  $\text{Na}^+$  gradients, and intracellular  $\text{Na}^+$  elevations can force astrocytic *GAT3* into the reverse mode, leading to a release of GABA (Wu et al., 2007; Richerson and Wu, 2003), which is sensed by microglial  $\text{GABA}_B$  receptors. We observed, in the present study, a delay in microglial versus astrocytic stimulation-evoked  $\text{Ca}^{2+}$  responses by, on average, 3.4 s, which is in the expected range of *GAT3* reversal. Although EAAT2 transporter currents occur within milliseconds after electrical stimulation (Srivastava et al., 2020), it takes between 0.9 s and 10 s until transporter-mediated, intra-astrocytic  $\text{Na}^+$  elevations reach their peak (Langer and Rose, 2009), which results in GABA release via the reversed GABA transport. The proposed mechanism is further supported by our observation that the microglial  $\text{Ca}^{2+}$  response is not affected by blocking glutamate receptors, both metabotropic and ionotropic, excluding an effect of the synaptically released glutamate on microglia via glutamate receptor activation. Indeed, microglial response rates to the application of external GABA exceeded those to electrical stimulation, most likely because the latter requires a local proximity of the (astrocytic) GABA release site and the responding microglial cells, whereas GABA application via the bath will activate all microglial  $\text{GABA}_B$  receptors.

Interestingly, microglial responses to neuronal stimulation only occurred at early postnatal ages and were completely absent in the adult. One possible explanation for this finding is that, in the immature brain, astrocytes provide a less tight synaptic ensheathment, which results in a more global spread of glutamate and leads to a more global increase of intracellular  $\text{Na}^+$  in the astrocytes. In the mature brain, synaptic enwrapment is confined to subcellular astrocytic structures as shown in the hippocampus and the cerebellum (Ventura and Harris, 1999; Bernardinelli et al., 2014). Another possibility is that a developmental change may affect astrocytic GABA transporter actions. *GAT3* co-transporters  $2\text{Na}^+$ ,  $1\text{Cl}^-$ , and 1GABA (Richerson and Wu, 2003), and the equilibrium depends on the intra- and extracellular concentrations of these components as well as the astrocytic membrane potential. There is good evidence that the cytosolic GABA concentration decreases in adult astrocytes (Ochi et al., 1993), probably because of a developmental drop in the GABA-synthesizing enzyme glutamic acid decarboxylase (GAD; Yoon and Lee, 2014), changes in alternative GABA metabolic pathways (Ishibashi et al., 2019; Schousboe et al., 2013), or less GABA uptake from extracellular space. Reduced intracellular GABA levels will decrease the probability of astrocytic *GAT3* to operate in reverse mode, which would explain the lack of microglial responses upon neuronal stimulation at adult stages. EAAT-mediated  $\text{Na}^+$  transients upon Schaffer collateral stimulation or external glutamate application are not significantly different between postnatal and adult astrocytes, excluding developmental changes in astrocytic  $\text{Na}^+$  homeostasis (Ziemens et al., 2019). Unfortunately, a comparative study about astrocytic intracellular  $\text{Na}^+$  and  $\text{Cl}^-$  concentrations at different developmental stages is presently not available. A third possible reason to explain the lack of microglial responses to electrical stimulation in the adult might be the developmentally distinct expression of EAAT isoforms. There is a significant increase in EAAT2 expression in hippocampal astrocytes during the first postnatal weeks, whereas EAAT1 expression does not alter (Clarke

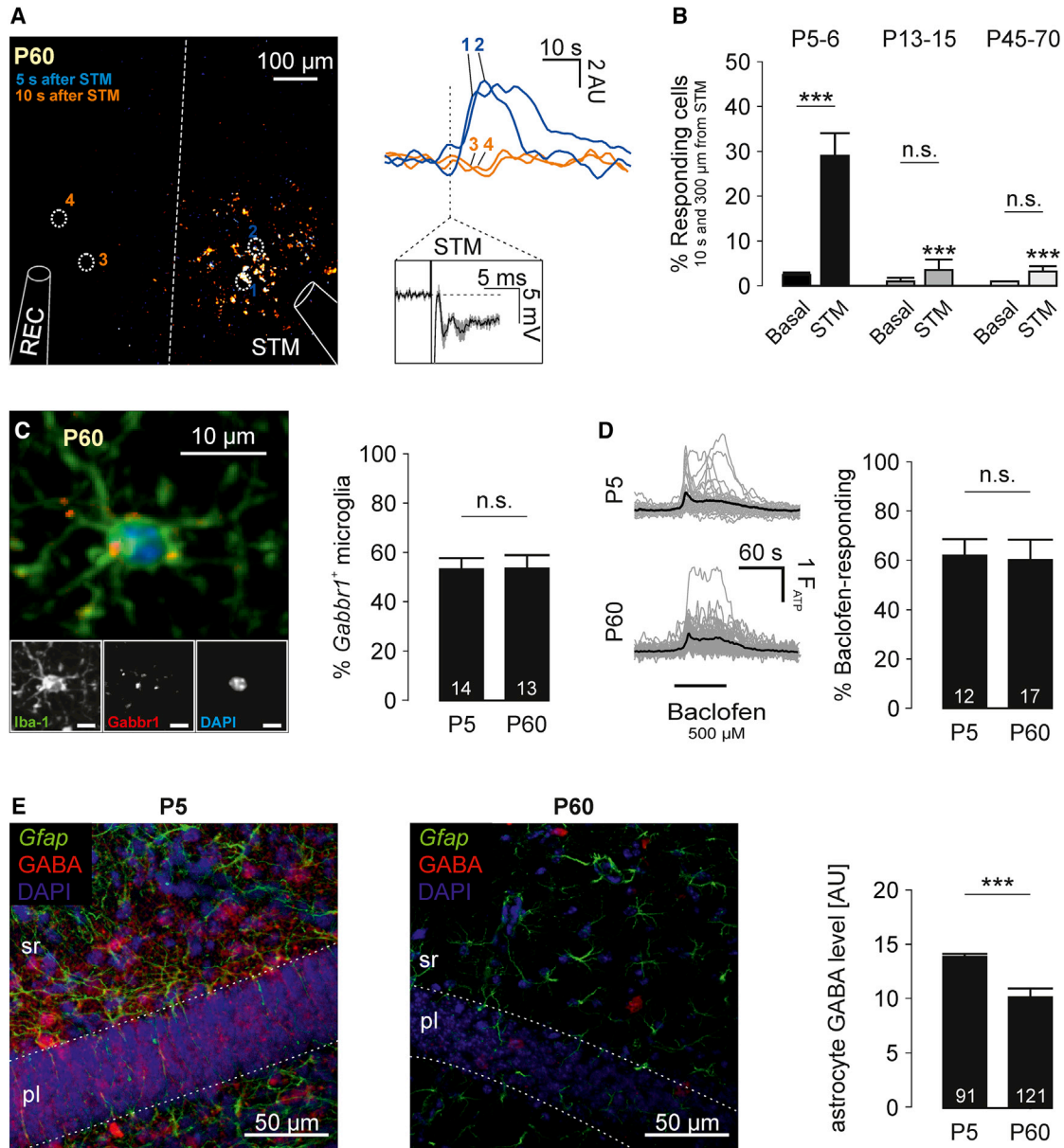


**Figure 7. Microglial responses upon electrical stimulation are only observed at early postnatal ages.**

(A) Left: two-photon microglial  $\text{Ca}^{2+}$  recording after electrical stimulation in a P60 C2G mouse. STM, stimulation pipette in CA3; REC, recording pipette in CA1. Signals in blue and orange indicate responses observed in 0–5 s and 5–10 s after the stimulus, respectively. White dashed line: 300  $\mu\text{m}$  distance from STM. Right: sample  $\text{Ca}^{2+}$  traces from ATP-responding microglial cells in adult brain slices close to the stimulation pipette (1, 2) and the recording pipette (3, 4). Scaling of amplitudes refers to an 8-bit range. Inset: field potential responses during STM. Scale bar: 100  $\mu\text{m}$ .

(B) Quantification of microglial  $\text{Ca}^{2+}$  responses after stimulation in neonatal (P5–P6;  $n = 21$  mice, 24 slices, 297 cells), juvenile (P13–P15;  $n = 3$  mice, 9 slices, 110 cells), and adult (P49–P70;  $n = 4$  mice, 7 slices, 55 cells) hippocampi. Data are presented as means  $\pm$  SEM. Statistical significance: n.s.,  $p \geq 0.05$ ; \*\*\* $p \leq 0.001$ .

(C) Left and middle: confocal images of a representative P60 microglial cell from CA1 stained for *Iba1* (green) and *Gabbr1* (red). DAPI channel is shown in blue. Right: quantification of stainings reveals similar *Gabbr1* expression in microglia at neonatal ( $n = 3$  mice, 15 slices) and adult stages ( $n = 3$  mice, 14 slices). Scale bar: 10  $\mu\text{m}$ .

(D) Left: microglial  $\text{Ca}^{2+}$  traces in neonatal ( $n = 5$  mice, 12 slices; 268 cells) and adult ( $n = 7$  mice, 26 slices; 263 cells) hippocampus before, during, and after external Baclofen (500  $\mu\text{M}$ ; bottom) application (gray). Black traces are the average of all gray traces. Amplitudes were normalized to the peak of the ATP response amplitude ( $=1 F_{\text{ATP}}$ ). Right: the percentage of CA1 microglia responding to Baclofen (500  $\mu\text{M}$ ) is not different between neonatal and adult.

(E) Left and middle: confocal images from stainings against *Gfap* (green) and GABA (red) in the CA1 region at P5 or P60. pl, pyramidal layer; sr, stratum radiatum. Scale bar: 50  $\mu\text{m}$ . Right: quantification of the GABA staining within *Gfap*<sup>+</sup> volume reveals an age-dependent decrease in astrocytic GABA load. Scale bar: 50  $\mu\text{m}$ . P5–P6:  $n = 3$  mice, 10 slices; P45–P70:  $n = 3$  mice, 12 slices.

et al., 2018). Concise studies about subcellular co-localization of GABA and glutamate transporters, however, still remain elusive, maybe because of technical limitations in the staining of a relatively few membrane-localized transporter proteins (Zhou and Danbolt, 2013). There is, hence, no evidence to support or to exclude the possibility that a developmental upregulation of EAAT2 might potentially be suppressive for reversing GAT3 action.

It is well known that developing neuronal networks in the hippocampus are initially formed by excitatory GABAergic connections and that during the first neonatal week, there is a shift toward glutamatergic signaling. In parallel, the functional roles of glial GABA seem to differ in the developing and the adult brain (Angulo et al., 2008). Indeed, as observed in *Drosophila* (Muthukumar et al., 2014), astrocyte development is tightly coupled with synaptogenesis, and shortly after synapse formation, the GABA transporter is upregulated in astrocytes depending on GABAergic neuronal activity and astrocytic GABA<sub>B</sub> receptor signaling, suggesting that astrocytes regulate GAT levels by direct measurement of extracellular GABA.

Intracellular Ca<sup>2+</sup> levels are critical for many microglial functions, such as motility, proliferation, and cytokine release (Färber and Kettenmann, 2006; Korvers et al., 2016; Pannell et al., 2014). Neuronal networks are formed by synapses, which transmit information to various brain regions and cell types. Synaptic formation in rodents starts during the early neonatal phase (Ben-Ari et al., 2007), in which synapses are initially overproduced, resulting in the pruning of synapses in an activity-dependent fashion (Paolicelli et al., 2011; Miyamoto et al., 2016). Microglia are involved in this developmental pruning process and complement receptors have been shown as important molecular determinants (Wilton et al., 2019). A very recent study demonstrated that around half of the cortical microglia population expresses GABA<sub>B</sub>R (Favuzzi et al., 2021) and that these microglia constitute a distinct population being more active with regard to synaptic pruning of inhibitory (GABAergic) synapses. We found, in the current study, similar expression levels of GABA<sub>B</sub> receptors in hippocampal microglia. Indeed, assuming that this pruning phenotype is also present in hippocampal tissue, our finding that there is no activity-dependence neuron-to-astrocyte-to-microglia communication in the adult, would get functional relevance in terms of developmental regulation of GABAergic synapse degradation.

Several previous studies described microglial Ca<sup>2+</sup> responses to changes in synaptic transmission by modulating overall neuronal activity using transgenic mouse models or inducing disease states (Umpierre et al., 2020; Umpierre and Wu, 2020; Liu et al., 2021; Eichhoff et al., 2011) and then analyzing changes in spontaneous microglial Ca<sup>2+</sup> signals. In the current study, we describe, for the first time, microglial Ca<sup>2+</sup> responses more directly, namely upon stimulation of neuronal signals. This sort of response was reliably induced but required a relatively high electrical stimulatory paradigm (at least 10 maximum pulses at 100 Hz). The reason may be due to a minimum of neurotransmitters that have to be released for a robust astrocytic GABA release, which is subsequently sensed by microglia. It has to be mentioned that, in physiology, such strong synaptic inputs will be barely apparent in healthy

developing tissue. However, the neuron-astrocyte-microglia communication via glutamate/GABA conversion could also be present under conditions that are below our stimulatory conditions and might be a regulator for microglial functions such as synaptic pruning.

In the present study, we present a tool to study microglia activity in the brain using Ca<sup>2+</sup> signaling as a readout. To study microglial Ca<sup>2+</sup> levels, synthetic dyes have been widely used for *in vitro* studies (Korvers et al., 2016; Pannell et al., 2014), whereas those tools are not applicable *in situ* or *in vivo* because of the difficulties of microglial cell dye-loading (Eichhoff et al., 2011; Brawek and Garaschuk, 2013). Recently, genetically encoded Ca<sup>2+</sup> indicators (GECI) based on variants of the green fluorescent protein have been used, and the sensor was delivered by various gene-delivery methods, such as viral infection or electroporation, which permitted recording Ca<sup>2+</sup> activity in brain slices or even in awake mice (Umpierre et al., 2020; Eichhoff et al., 2011; Seifert et al., 2011). However, these gene-delivery methods are invasive and provide non-homogeneous and non-stationary expression. Furthermore, they are hardly applicable to neonatal mice. The microglial Ca<sup>2+</sup> indicator mouse models (C2G and C2M2G) overcome all these difficulties because they do not depend on any Cre recombinase activation or viruses. Additionally, they use one of the newest generations of GCaMP6 sensors (GCaMP6m), which responds to transient increases in intracellular Ca<sup>2+</sup> with large changes in fluorescence intensity (Barnett et al., 2017). Furthermore, GCaMP6m expression is—at all investigated ages—strongly restricted to microglial cells, with no expression in other cell types. The microglia-specific indicator mouse models are, therefore, suitable tools to further investigate the involvement of microglia in pan-glial and neuron-glia communication in the brain.

## LIMITATIONS OF THE STUDY

We report a neuron-astrocyte-microglia communication via glutamate and GABA in the early postnatal hippocampus. This pathway is only present at early developmental stages, and the reason for its absence in the adult was not fully addressed. We demonstrate that the intracellular astrocytic GABA load changes upon brain development and present this as a possible explanation for a lack in GABA transporter reversal and, thus, microglia Ca<sup>2+</sup> responses to electrical stimulation. Further experimental approaches, such as ELISA for GABA or employing GABA-sensitive electrodes, would strengthen the statement of developmental changes in astrocytic GABA load. Further experimental approaches with manipulations of that astrocytic internal GABA load are needed to prove that microglial responses to Schaffer collateral pathway stimulation correlate with astrocytic GABA levels. A further limitation of this study is that no evidence was provided for a statement on the functional relevance of the reported STM-evoked Ca<sup>2+</sup> elevations on microglial actions, e.g., synaptic pruning. Further studies might clarify this issue, e.g., by using cell-type-specific KO mouse models for GABA<sub>B</sub> receptors or GAT3. The study is also limited to microglial and astrocytic Ca<sup>2+</sup> elevations—future studies might also include changes in intracellular cAMP and Na<sup>+</sup> levels.

## STAR★METHODS

Detailed methods are provided in the online version of this paper and include the following:

- KEY RESOURCES TABLE
- RESOURCE AVAILABILITY
  - Lead contact
  - Materials availability
  - Data and code availability
- EXPERIMENTAL MODEL AND SUBJECT DETAILS
  - Ethics statement
  - Mice
  - C2M2G: Csf1r-2A-mCherry-2A-GCaMP6m
- METHOD DETAILS
  - Generation of transgenic mice
  - Immunohistochemistry and confocal microscopy
  - Acute brain slice preparation
  - *In situ* Ca<sup>2+</sup> imaging
  - Electrical stimulation
- QUANTIFICATION AND STATISTICAL ANALYSIS
  - Quantification of immunohistochemical stainings
  - Data analysis of Ca<sup>2+</sup> imaging movies

## SUPPLEMENTAL INFORMATION

Supplemental information can be found online at <https://doi.org/10.1016/j.celrep.2021.110128>.

## ACKNOWLEDGMENTS

We are grateful to Regina Piske, Nadine Scharek, Maren Wendt, Andrea Leschke, Bastiaan Pierik, Matthias Richter, and Christine Molenda (Advanced Light Microscopy) for technical assistance and to Dr. Alice Buonfiglioli and Dr. Niccolò Pampaloni for data discussion. This work was supported by the Helmholtz-Gemeinschaft, Zukunftsthema “Immunology and Inflammation” (ZT-0027), and by the Einstein-Stiftung.

## AUTHOR CONTRIBUTIONS

F.L., P.X., S.V.G., C.F., Y.-J.C., and M.S. performed the calcium imaging experiments; F.L. performed Schaffer collateral stimulations; F.L. and M.S. performed confocal microscopy and analysis; A.S. helped to perform calcium imaging on microglial processes; B.U. performed additional experiments during the execution of this project; M.S. and R.K. generated the transgenic mouse models; M.S. performed the meta-analysis of transcriptomic data; F.L., H.K., and M.S. wrote the first draft of the manuscript and prepared the figures; F.L., H.K., and M.S. supervised the trainees (S.V.G., C.F., and Y.-J.C.) who participated in performing the experiments; M.S., F.L., and H.K. designed the experiments; H.K. and M.S. oversaw the studies, mentored the trainees, and revised the manuscript; and H.K. provided funding for this project.

## DECLARATION OF INTERESTS

P.X., S.V.G., C.F., and Y.-J.C. worked as students on this project in our MDC team. For convenience, we did not state all their home university affiliations, and we did not include all their current affiliations. The authors declare no further competing interests.

Received: February 26, 2021  
Revised: September 14, 2021  
Accepted: November 22, 2021  
Published: December 28, 2021

## SUPPORTING CITATIONS

The following references appear in the supplemental information: Bennett et al. (2016); Sakaba and Neher (2003); Thanawala and Regehr (2013); Valente et al. (2017).

## REFERENCES

- Angulo, M.C., Le Meur, K., Kozlov, A.S., Charpak, S., and Audinat, E. (2008). GABA, a forgotten gliotransmitter. *Prog. Neurobiol.* *86*, 297–303.
- Barnett, L.M., Hughes, T.E., and Drobizhev, M. (2017). Deciphering the molecular mechanism responsible for GCaMP6m's Ca<sup>2+</sup>-dependent change in fluorescence. *PLoS ONE* *12*, e0170934.
- Ben-Ari, Y., Gaiarsa, J.L., Tyzio, R., and Khazipov, R. (2007). GABA: A pioneer transmitter that excites immature neurons and generates primitive oscillations. *Physiol. Rev.* *87*, 1215–1284.
- Bennett, M.L., Bennett, F.C., Liddel, S.A., Ajami, B., Zamanian, J.L., Fernhoff, N.B., Mulinyawe, S.B., Bohlen, C.J., Adil, A., Tucker, A., et al. (2016). New tools for studying microglia in the mouse and human CNS. *Proc. Natl. Acad. Sci. USA* *113*, E1738–E1746.
- Bernardinelli, Y., Randall, J., Janett, E., Nikonenko, I., König, S., Jones, E.V., Flores, C.E., Murai, K.K., Bochet, C.G., Holtmaat, A., and Müller, D. (2014). Activity-dependent structural plasticity of perisynaptic astrocytic domains promotes excitatory synapse stability. *Curr. Biol.* *24*, 1679–1688.
- Borden, L.A. (1996). GABA transporter heterogeneity: Pharmacology and cellular localization. *Neurochem. Int.* *29*, 335–356.
- Boucsein, C., Zacharias, R., Färber, K., Pavlovic, S., Hanisch, U.K., and Kettenmann, H. (2003). Purinergic receptors on microglial cells: Functional expression in acute brain slices and modulation of microglial activation *in vitro*. *Eur. J. Neurosci.* *17*, 2267–2276.
- Brawek, B., and Garaschuk, O. (2013). Microglial calcium signaling in the adult, aged and diseased brain. *Cell Calcium* *53*, 159–169.
- Brawek, B., Schwendele, B., Riester, K., Kohsaka, S., Lerdkrai, C., Liang, Y., and Garaschuk, O. (2014). Impairment of *in vivo* calcium signaling in amyloid plaque-associated microglia. *Acta Neuropathol.* *127*, 495–505.
- Brawek, B., Liang, Y., Savitska, D., Li, K., Fomin-Thunemann, N., Kovalchuk, Y., Zirdum, E., Jakobsson, J., and Garaschuk, O. (2017). A new approach for ratiometric *in vivo* calcium imaging of microglia. *Sci. Rep.* *7*, 6030.
- Chechik, G., Meilijson, I., and Ruppin, E. (1998). Synaptic pruning in development: A computational account. *Neural Comput.* *10*, 1759–1777.
- Clapham, D.E. (2007). Calcium signaling. *Cell* *131*, 1047–1058.
- Clarke, L.E., Liddel, S.A., Chakraborty, C., Münch, A.E., Heiman, M., and Barres, B.A. (2018). Normal aging induces A1-like astrocyte reactivity. *Proc. Natl. Acad. Sci. USA* *115*, E1896–E1905.
- Davalos, D., Grutzendler, J., Yang, G., Kim, J.V., Zuo, Y., Jung, S., Littman, D.R., Dustin, M.L., and Gan, W.B. (2005). ATP mediates rapid microglial response to local brain injury *in vivo*. *Nat. Neurosci.* *8*, 752–758.
- Divito, C.B., and Underhill, S.M. (2014). Excitatory amino acid transporters: Roles in glutamatergic neurotransmission. *Neurochem. Int.* *73*, 172–180.
- Eichhoff, G., Brawek, B., and Garaschuk, O. (2011). Microglial calcium signal acts as a rapid sensor of single neuron damage *in vivo*. *Biochim. Biophys. Acta* *1813*, 1014–1024.
- Eyo, U.B., Peng, J., Swiatkowski, P., Mukherjee, A., Bispo, A., and Wu, L.J. (2014). Neuronal hyperactivity recruits microglial processes via neuronal NMDA receptors and microglial P2Y12 receptors after status epilepticus. *J. Neurosci.* *34*, 10528–10540.
- Färber, K., and Kettenmann, H. (2006). Functional role of calcium signals for microglial function. *Glia* *54*, 656–665.
- Favuzzi, E., Huang, S., Saldi, G.A., Binan, L., Ibrahim, L.A., Fernández-Otero, M., Cao, Y., Zeine, A., Sefah, A., Zheng, K., et al. (2021). GABA-receptive microglia selectively sculpt developing inhibitory circuits. *Cell* *184*, 4048–4063.e32.

- Gee, J.M., Smith, N.A., Fernandez, F.R., Economo, M.N., Brunert, D., Rothermel, M., Morris, S.C., Talbot, A., Palumbos, S., Ichida, J.M., et al. (2014). Imaging activity in neurons and glia with a Polr2a-based and cre-dependent GCaMP5G-IRES-tdTomato reporter mouse. *Neuron* 83, 1058–1072.
- Haydon, P.G., and Carmignoto, G. (2006). Astrocyte control of synaptic transmission and neurovascular coupling. *Physiol. Rev.* 86, 1009–1031.
- Héja, L., Nyitrai, G., Kékesi, O., Dobolyi, A., Szabó, P., Fiáth, R., Ulbert, I., Pál-Szenthe, B., Palkovits, M., and Kardos, J. (2012). Astrocytes convert network excitation to tonic inhibition of neurons. *BMC Biol.* 10, 26.
- Ishibashi, M., Egawa, K., and Fukuda, A. (2019). Diverse actions of astrocytes in GABAergic signaling. *Int. J. Mol. Sci.* 20, 2964.
- Kettenmann, H., Hanisch, U.K., Noda, M., and Verkhratsky, A. (2011). Physiology of microglia. *Physiol. Rev.* 91, 461–553.
- Kettenmann, H., Kirchhoff, F., and Verkhratsky, A. (2013). Microglia: New roles for the synaptic stripper. *Neuron* 77, 10–18.
- Korvers, L., de Andrade Costa, A., Mersch, M., Matyash, V., Kettenmann, H., and Semtner, M. (2016). Spontaneous Ca<sup>2+</sup> transients in mouse microglia. *Cell Calcium* 60, 396–406.
- Krabbe, G., Matyash, V., Pannasch, U., Mamer, L., Boddeke, H.W., and Kettenmann, H. (2012). Activation of serotonin receptors promotes microglial injury-induced motility but attenuates phagocytic activity. *Brain Behav. Immun.* 26, 419–428.
- Kuhn, S.A., van Landeghem, F.K., Zacharias, R., Färber, K., Rappert, A., Pavlovic, S., Hoffmann, A., Nolte, C., and Kettenmann, H. (2004). Microglia express GABA<sub>B</sub> receptors to modulate interleukin release. *Mol. Cell. Neurosci.* 25, 312–322.
- Langer, J., and Rose, C.R. (2009). Synaptically induced sodium signals in hippocampal astrocytes *in situ*. *J. Physiol.* 587, 5859–5877.
- Liu, L., Kearns, K.N., Eli, I., Sharifi, K.A., Soldo, S., Carlson, E.W., Scott, K.W., Sluzewski, M.F., Acton, S.T., Stauderman, K.A., et al. (2021). Microglial calcium waves during the hyperacute phase of ischemic stroke. *Stroke* 52, 274–283.
- Mariotti, L., Losi, G., Sessolo, M., Marcon, I., and Carmignoto, G. (2016). The inhibitory neurotransmitter GABA evokes long-lasting Ca<sup>2+</sup> oscillations in cortical astrocytes. *Glia* 64, 363–373.
- Michell-Robinson, M.A., Touil, H., Healy, L.M., Owen, D.R., Durafourt, B.A., Bar-Or, A., Antel, J.P., and Moore, C.S. (2015). Roles of microglia in brain development, tissue maintenance and repair. *Brain* 138, 1138–1159.
- Miyamoto, A., Wake, H., Ishikawa, A.W., Eto, K., Shibata, K., Murakoshi, H., Koizumi, S., Moorhouse, A.J., Yoshimura, Y., and Nabekura, J. (2016). Microglia contact induces synapse formation in developing somatosensory cortex. *Nat. Commun.* 7, 12540.
- Muthukumar, A.K., Stork, T., and Freeman, M.R. (2014). Activity-dependent regulation of astrocyte GAT levels during synaptogenesis. *Nat. Neurosci.* 17, 1340–1350.
- Nimmerjahn, A., Kirchhoff, F., and Helmchen, F. (2005). Resting microglial cells are highly dynamic surveillants of brain parenchyma *in vivo*. *Science* 308, 1314–1318.
- Ochi, S., Lim, J.Y., Rand, M.N., During, M.J., Sakatani, K., and Kocsis, J.D. (1993). Transient presence of GABA in astrocytes of the developing optic nerve. *Glia* 9, 188–198.
- Panatier, A., Theodosis, D.T., Mothet, J.P., Touquet, B., Pollegioni, L., Poulain, D.A., and Oliet, S.H. (2006). Glia-derived D-serine controls NMDA receptor activity and synaptic memory. *Cell* 125, 775–784.
- Pannell, M., Szulzewsky, F., Matyash, V., Wolf, S.A., and Kettenmann, H. (2014). The subpopulation of microglia sensitive to neurotransmitters/neurohormones is modulated by stimulation with LPS, interferon- $\gamma$ , and IL-4. *Glia* 62, 667–679.
- Pannell, M., Meier, M.A., Szulzewsky, F., Matyash, V., Endres, M., Kronenberg, G., Prinz, V., Waiczies, S., Wolf, S.A., and Kettenmann, H. (2016). The subpopulation of microglia expressing functional muscarinic acetylcholine receptors expands in stroke and Alzheimer's disease. *Brain Struct. Funct.* 221, 1157–1172.
- Paolicelli, R.C., Bolasco, G., Pagani, F., Maggi, L., Scianni, M., Panzanelli, P., Giustetto, M., Ferreira, T.A., Guiducci, E., Dumas, L., et al. (2011). Synaptic pruning by microglia is necessary for normal brain development. *Science* 333, 1456–1458.
- Pascual, O., Ben Achour, S., Rostaing, P., Triller, A., and Bessis, A. (2012). Microglia activation triggers astrocyte-mediated modulation of excitatory neurotransmission. *Proc. Natl. Acad. Sci. USA* 109, E197–E205.
- Patel, S., and Player, M.R. (2009). Colony-stimulating factor-1 receptor inhibitors for the treatment of cancer and inflammatory disease. *Curr. Top. Med. Chem.* 9, 599–610.
- Pocock, J.M., and Kettenmann, H. (2007). Neurotransmitter receptors on microglia. *Trends Neurosci.* 30, 527–535.
- Pozner, A., Xu, B., Palumbos, S., Gee, J.M., Tvrdik, P., and Capecci, M.R. (2015). Intracellular calcium dynamics in cortical microglia responding to focal laser injury in the PC:G5-tdT reporter mouse. *Front. Mol. Neurosci.* 8, 12.
- Richerson, G.B., and Wu, Y. (2003). Dynamic equilibrium of neurotransmitter transporters: Not just for reuptake anymore. *J. Neurophysiol.* 90, 1363–1374.
- Rose, C.R., Felix, L., Zeug, A., Dietrich, D., Reiner, A., and Henneberger, C. (2018). Astroglial glutamate signaling and uptake in the hippocampus. *Front. Mol. Neurosci.* 10, 451.
- Sakaba, T., and Neher, E. (2003). Direct modulation of synaptic vesicle priming by GABA<sub>B</sub> receptor activation at a glutamatergic synapse. *Nature* 424, 775–778.
- Schafer, D.P., Lehrman, E.K., Kautzman, A.G., Koyama, R., Mardinly, A.R., Yasumaki, R., Ransohoff, R.M., Greenberg, M.E., Barres, B.A., and Stevens, B. (2012). Microglia sculpt postnatal neural circuits in an activity and complement-dependent manner. *Neuron* 74, 691–705.
- Schafer, D.P., Lehrman, E.K., and Stevens, B. (2013). The “quad-partite” synapse: microglia-synapse interactions in the developing and mature CNS. *Glia* 61, 24–36.
- Schipke, C.G., Boucsein, C., Ohlemeyer, C., Kirchhoff, F., and Kettenmann, H. (2002). Astrocyte Ca<sup>2+</sup> waves trigger responses in microglial cells in brain slices. *FASEB J.* 16, 255–257.
- Schousboe, A., Bak, L.K., and Waagepetersen, H.S. (2013). Astrocytic control of biosynthesis and turnover of the neurotransmitters glutamate and GABA. *Front. Endocrinol. (Lausanne)* 4, 102.
- Seifert, S., Pannell, M., Uckert, W., Färber, K., and Kettenmann, H. (2011). Transmitter- and hormone-activated Ca<sup>2+</sup> responses in adult microglia/brain macrophages *in situ* recorded after viral transduction of a recombinant Ca<sup>2+</sup> sensor. *Cell Calcium* 49, 365–375.
- Shigeri, Y., Seal, R.P., and Shimamoto, K. (2004). Molecular pharmacology of glutamate transporters, EAATs and VGLUTs. *Brain Res. Brain Res. Rev.* 45, 250–265.
- Shigetomi, E., Hirayama, Y.J., Ikenaka, K., Tanaka, K.F., and Koizumi, S. (2018). Role of purinergic receptor P2Y1 in spatiotemporal Ca<sup>2+</sup> dynamics in astrocytes. *J. Neurosci.* 38, 1383–1395.
- Srivastava, I., Vazquez-Juarez, E., and Lindskog, M. (2020). Reducing glutamate uptake in rat hippocampal slices enhances astrocytic membrane depolarization while down-regulating CA3-CA1 synaptic response. *Front. Synaptic Neurosci.* 12, 37.
- Tabula Muris Consortium (2018). Single-cell transcriptomics of 20 mouse organs creates a *Tabula Muris*. *Nature* 562, 367–372.
- Thanawala, M.S., and Regehr, W.G. (2013). Presynaptic calcium influx controls neurotransmitter release in part by regulating the effective size of the readily releasable pool. *J. Neurosci.* 33, 4625–4633.
- Tremblay, M.E., Stevens, B., Sierra, A., Wake, H., Bessis, A., and Nimmerjahn, A. (2011). The role of microglia in the healthy brain. *J. Neurosci.* 31, 16064–16069.
- Tsukada, S., Iino, M., Takayasu, Y., Shimamoto, K., and Ozawa, S. (2005). Effects of a novel glutamate transporter blocker, (2S, 3S)-3-[3-[4-(trifluoromethyl)benzoylamino]benzyloxy]aspartate (TFB-TBOA), on activities of hippocampal neurons. *Neuropharmacology* 48, 479–491.

- Umpierre, A.D., Bystrom, L.L., Ying, Y., Liu, Y.U., Worrell, G., and Wu, L.J. (2020). Microglial calcium signaling is attuned to neuronal activity in awake mice. *eLife* 9, e56502.
- Umpierre, A.D., and Wu, L.J. (2020). How microglia sense and regulate neuronal activity. *Glia* 69, 1637–1653.
- Valente, P., Farisello, P., Valtorta, F., Baldelli, P., and Benfenati, F. (2017). Impaired GABA<sub>B</sub>-mediated presynaptic inhibition increases excitatory strength and alters short-term plasticity in synapsin knockout mice. *Oncotarget* 8, 90061–90076.
- Ventura, R., and Harris, K.M. (1999). Three-dimensional relationships between hippocampal synapses and astrocytes. *J. Neurosci.* 19, 6897–6906.
- Volterra, A., and Meldolesi, J. (2005). Astrocytes, from brain glue to communication elements: The revolution continues. *Nat. Rev. Neurosci.* 6, 626–640.
- Wake, H., Moorhouse, A.J., Jinno, S., Kohsaka, S., and Nabekura, J. (2009). Resting microglia directly monitor the functional state of synapses *in vivo* and determine the fate of ischemic terminals. *J. Neurosci.* 29, 3974–3980.
- Wake, H., Moorhouse, A.J., Miyamoto, A., and Nabekura, J. (2013). Microglia: Actively surveying and shaping neuronal circuit structure and function. *Trends Neurosci.* 36, 209–217.
- Wilton, D.K., Dissing-Olesen, L., and Stevens, B. (2019). Neuron-glia signaling in synapse elimination. *Annu. Rev. Neurosci.* 42, 107–127.
- Wu, Y., Wang, W., Díez-Sampedro, A., and Richerson, G.B. (2007). Nonvesicular inhibitory neurotransmission via reversal of the GABA transporter GAT-1. *Neuron* 56, 851–865.
- Yoon, B.-E., and Lee, C.J. (2014). GABA as a rising gliotransmitter. *Front. Neural Circuits* 8, 141.
- Zhang, Y., Chen, K., Sloan, S.A., Bennett, M.L., Scholze, A.R., O’Keeffe, S., Phatnani, H.P., Guarnieri, P., Caneda, C., Ruderisch, N., et al. (2014). An RNA-sequencing transcriptome and splicing database of glia, neurons, and vascular cells of the cerebral cortex. *J. Neurosci.* 34, 11929–11947.
- Zhou, Y., and Danbolt, N.C. (2013). GABA and glutamate transporters in brain. *Front. Endocrinol. (Lausanne)* 4, 165.
- Ziemens, D., Oschmann, F., Gerkau, N.J., and Rose, C.R. (2019). Heterogeneity of activity-induced sodium transients between astrocytes of the mouse hippocampus and neocortex: Mechanisms and consequences. *J. Neurosci.* 39, 2620–2634.

STAR★METHODS

KEY RESOURCES TABLE

REAGENT OR RESOURCE	SOURCE	IDENTIFIER
<b>Antibodies</b>		
Goat anti-iba1	Abcam	cat# ab5076; RRID: AB_2224402
Chicken anti-gfp	Abcam	cat# ab13970; RRID: AB_300798
Rabbit anti-rfp	Rockland Immunochemicals	cat# 600-401-379; RRID: AB_2209751
Guinea pig anti-gaba	Abcam	cat# ab17413; RRID: AB_443865
Mouse anti-neun	Synaptic Systems	cat# 266 004; RRID: AB_2619988
Rabbit anti-gabbr1	Chemicon international	cat# AB5850; RRID: AB_11212717
Rabbit anti-gfap	Synaptic Systems	cat# Z0334; RRID: AB_10013382
Guinea pig anti-gfap	Synaptic Systems	cat# 173 004; RRID: AB_10641162
Donkey anti-goat igg; cy5	Dianova	cat# 705-175-147; RRID: AB_2340415
Donkey anti-chicken igg (h+I); alexa488	Dianova	cat# 703-545-155; RRID: AB_2340375
Donkey anti-rabbit igg (h+I); cy3	Dianova	cat# 711-165-152; RRID: AB_2307443
Donkey anti-guinea pig igg (h+I); cy5	Dianova	cat# 706-605-148; RRID: AB_2340476
Donkey anti-mouse igg (h+I); cy3	Dianova	cat# 715-165-150; RRID: AB_2340813
Donkey anti-guinea pig igg (h+I); dylight 405	Dianova	cat# 706-475-148; RRID: AB_2340470
Dapi	Dianova	cat# 32670; RRID: AB_2173853
<b>Chemicals, peptides, and recombinant proteins</b>		
Aqua-poly/mount	Polysciences	cat#18606-5
Adenosine 5'-triphosphate disodium salt hydrate	Sigma-Aldrich	cat# 34369-07-8
L-glutamic acid sodium salt hydrate	Sigma-Aldrich	cat# 142-47-2
Ly379268	Tocris	cat# 2453/10
Tetrodotoxin (ttx)	AdooQ Biosciences	cat# 1078/1
Γ-aminobutyric acid (gaba)	Sigma-Aldrich	cat# 0344/1G
R <sup>+</sup> -baclofen hydrochloride	Sigma-Aldrich	cat# 63701-55-3
DI-2-amino-3-phosphonopropionic acid (d-ap3)	Tocris	cat# 0125/100
Ly341495	Tocris	cat# 1209/1
(2s, 3s)-3-[3-[4-(trifluoromethyl)benzoylamino] benzyloxy]aspartate (tfb-tboa)	Tocris	cat# 2532
Cyclopropyl-4-phosphonophenylglycine (cppg)	Tocris	cat# 0972/5
6-cyano-7-nitroquinoxaline-2,3-dione (cnqx)	Tocris	cat# 1045/1
2-amino-5-phosphonopentanoic acid (apv)	Tocris	cat# 0106/1
Picrotoxin	Tocris	cat# 1128
Guvacine	Tocris	cat# 0234
Snap5114	Sigma-Aldrich	cat# 157604-55-2
D-aspartic acid	Sigma-Aldrich	cat# 1783-96-6
Kainic acid	Tocris	cat# 0222/1
Methyl-d-aspartic acid (nmda)	Sigma-Aldrich	cat# 6384-92-5
Ar-c69931 tetrasodium salt	Tocris	cat# 5720
Muscimol	Tocris	cat# 0289/1

(Continued on next page)

**Continued**

REAGENT OR RESOURCE	SOURCE	IDENTIFIER
<b>Experimental models: Organisms/strains</b>		
Mouse: csf1r-2a-gcamp6m	Transgenic Core Facility of the Max Delbrück Center	N/A
Mouse: csf1r-2a-mc-2a-gcamp6m	Transgenic Core Facility of the Max Delbrück Center	N/A
<b>Oligonucleotides</b>		
Csf1r-gcamp_gforw (aactcagctgttctggcttc)		N/A
Csf1r -gcamp_grevwt (cccctcatgttctgaagtgtca)		N/A
Csf1r -gcamp_grevmut (ggtgttctgctgtagtggt)		N/A
Csf1r_mc_gcamp_rev (ttcagcttgccggtctgggtg)		N/A
<b>Software and algorithms</b>		
Tida 5.25	HEKA Electronics	N/A
Thorimage 8.0	Thorlabs	<a href="https://www.thorlabs.de/newgrouppage9.cfm?objectgroup_id=9072&amp;tabname=Specifications#ad-image-0">https://www.thorlabs.de/newgrouppage9.cfm?objectgroup_id=9072&amp;tabname=Specifications#ad-image-0</a>
Igor pro 6.37	WaveMetrics	<a href="https://www.wavemetrics.com/products/igorpro">https://www.wavemetrics.com/products/igorpro</a>
Graphpad prism 7	La Jolla	<a href="https://www.graphpad.com/scientific-software/prism/">https://www.graphpad.com/scientific-software/prism/</a>
<b>Other</b>		
Hm650v vibratome	Thermo Scientific	cat#10076838
Epc9 or Epc10 amplifier	HEKA Elektronik	N/A
Leica tcs spe upright confocal laser scanning microscope	Leica Microsystem	N/A
Axioscope 2 fs plus	Carl Zeiss Microscopy GmbH	N/A
Polychrome iv	Till Photonics	N/A
Zyla 5.5 camera	Oxford Instruments	N/A
Chameleon ultra ii laser	Coherent	N/A
Gaasp photomultipliers	Thorlabs	<a href="https://www.thorlabs.de/newgrouppage9.cfm?objectgroup_id=2909">https://www.thorlabs.de/newgrouppage9.cfm?objectgroup_id=2909</a>
Zeiss lsm 880 nlo with fast airyscan	Carl Zeiss Microscopy GmbH	<a href="https://www.zeiss.com/microscopy/int/dynamic-content/news/2014/news-lsm-880.html">https://www.zeiss.com/microscopy/int/dynamic-content/news/2014/news-lsm-880.html</a>
Fiji imagej	NIH	<a href="https://imagej.net/software/fiji/downloads">https://imagej.net/software/fiji/downloads</a>

**RESOURCE AVAILABILITY**

**Lead contact**

Further information and requests for resources and reagents should be directed to and will be fulfilled by the lead contact, Marcus Semtner, PhD ([marcus.semtner@mdc-berlin.de](mailto:marcus.semtner@mdc-berlin.de)).

**Materials availability**

Mouse lines generated in this study are available on request by the lead contact ([marcus.semtner@mdc-berlin.de](mailto:marcus.semtner@mdc-berlin.de)).

**Data and code availability**

- All data reported in this paper will be shared by the lead contact upon request.
- All original code is available in this paper's [supplemental information](#).
- Any additional information required to reanalyze the data reported in this paper is available from the lead contact upon request.

## EXPERIMENTAL MODEL AND SUBJECT DETAILS

### Ethics statement

This study was carried out at the Max Delbrück Center for Molecular Medicine (MDC) in accordance with all the internal guidelines. All procedures involving handling of living animals were performed in strict accordance with the European directive (2010/63/UE), the German Animal Protection Law, and were approved by the Regional Office for Health and Social Services in Berlin (Landesamt für Gesundheit und Soziales, Berlin, Germany, Permit Number G0111/17, T0014/08, X9023/12, X9005/18, A0376/17). Mice were housed in standard cages in a specific pathogen-free facility on a 12h light/dark cycle with *ad libitum* access to food and water. For preparation of acute brain slices, adult and juvenile mice were euthanized by cervical dislocation. Neonatal mice were sacrificed by direct decapitation using surgical scissors. For immunohistochemistry, all the mice were sacrificed by deep anesthesia and perfusion fixation. All efforts were made to minimize suffering.

### Mice

#### C2G: *Csf1r-2A-GCaMP6m*

Description: C2G bears cytosolic expression of the Ca<sup>2+</sup>-sensitive protein GCaMP6m in microglia

Permission: Landesamt für Gesundheit und Soziales, Berlin, Germany, Permit Number G0111/17, T0014/08, X9023/12, X9005/18, A0376/17

Species: Mouse (Bl6/N)

Maintenance: standard cages in a specific pathogen-free facility on a 12h light/dark cycle with *ad libitum* access to food and water

Age: P5-7, P13-15, P40-70, as indicated in the text

Sex: Experimental groups were composed by equal numbers of male and female mice. Male and female data were pooled as no differences were found in the microglial responses to STM and to ATP.

#### C2M2G: *Csf1r-2A-mCherry-2A-GCaMP6m*

Description: C2G bears cytosolic expression of the Ca<sup>2+</sup>-sensitive protein GCaMP6m and mCherry in microglia

Permission: Landesamt für Gesundheit und Soziales, Berlin, Germany, Permit Number G0111/17, T0014/08, X9023/12, X9005/18, A0376/17

Species: Mouse (Bl6/N)

Maintenance: standard cages in a specific pathogen-free facility on a 12h light/dark cycle with *ad libitum* access to food and water

Age: P5-7, P13-15, P40-70, as indicated in the text

Sex: Experimental groups were composed by equal numbers of male and female mice. Male and female data were pooled as no differences were found in the microglial responses to STM and to ATP.

## METHOD DETAILS

### Generation of transgenic mice

Wild-type C57BL/6 mice were provided by Charles River Laboratories (Sulzfeld, Germany). Based on this genetic background, we generated two transgenic mouse lines *Csf1r-2A-GCaMP6m* (C2G) and *csf1r-2A-mCherry-2A-GCaMP6m* (C2M2G). The GCaMP6m sensor is constructed with circularly-permuted green fluorescent protein (GFP) and its sequence is linked by the 2A self-cleaving peptide with the microglial colony stimulating factor 1 receptor (*Csf1r*) promoter sequence. *Csf1R* is a lineage-restricted receptor for proper proliferation, differentiation and survival of microglia (Patel and Player, 2009). The transgenic mouse construct thus was developed with *Csf1r* sequence inserted in its promoter region, allowing the reporter GCaMP6m Ca<sup>2+</sup> sensor to be specifically expressed by microglia in the central nervous system. C2G and C2M2G transgenic mice were generated at the Transgenic Core Facility of the MDC, Berlin (TCF) using the CRISPR/Cas9 technology and insertion of a large fragment by homology-directed repair. Cas9 protein was obtained from IDT (Leuven, Belgium). gRNAs were designed manually, *in silico* validated on <http://crispor.tefor.net> and ordered as crRNA from IDT. The donor vector was synthesized by Biomatik (Kitchener, Canada) and was based on a puC57 backbone containing the genomic sequences 1200 bp upstream and 1500 bp downstream of the *csf1r* stop codon as well as the 2A-GCaMP6m (C2G) or 2A-mCherry-2A-GCaMP6m (C2M2G) cassettes. Thus, the genetic information of the cytosolic fluorescent Ca<sup>2+</sup> indicator protein GCaMP6m was introduced at the C-terminal end of the *csf1r* gene, immediately before the STOP codon. Cas9 mRNA, sgRNAs and donor vector were injected into zygotes which were subsequently cultured for 1 day and then implanted into a surrogate mother animal.

The successful insertion of transgenic regions was tested by genotyping using the combination of the following primers: *Csf1R-GCaMP\_gforw* (5'-AACTTCAGCTGTTTCTGGCTTC), *Csf1R-GCaMP\_grevWT* (5'-CCCCTCATGTTCTGAAGTGTCA) as well as *Csf1R-GCaMP\_grevMut* (5'-GGTGTCTGCTGGTAGTGGT) or *Csf1R\_mC\_Gcamp\_rev* (5'-TTCAGCTTGGCGGTCTGGGTG) for C2G or C2M2G, respectively. Genotyping PCRs yielded a 344 bp band for the WT allele, a 457 bp band for the C2G allele and a 429 bp band for the C2M2G allele. In the case of the C2G line, we got 19 pups from 4 independent approaches; 3 of the pups

were homozygous, and another 3 were heterozygous for GCaMP6m. In a parallel approach, we used a similar strategy to introduce the larger 2A-mCherry-2A-GCaMP6m cassette at the C terminus of the endogenous *csf1r* gene (Figure 1B), leading to mice which express the mCherry fluorescence reporter in addition to GCaMP6m specifically in microglia. From the latter one, we got 25 pups from 4 approaches; 1 of them was homozygous, and another 4 were heterozygous for the mCherry-2A-GCaMP6m transgenic allele. The phenotypic appearance, fertility, breeding, and exploration behavior, motility and lifespan expectation could not be distinguished from wild-type B6 mice, suggesting that the two mouse lines do not suffer from the reporter insertions. The successful generation of the GCaMP6m transgenic animals was also confirmed by immunohistochemistry and confocal microscopy (see below). All animals were maintained at the Max Delbrück Center's animal facility, kept under a 12h/12h dark/light cycle with food and water supply *ad libitum*, until used for *in situ* Ca<sup>2+</sup> imaging or immunohistochemistry experiments. Both male and female animals were used in this study. Although C2G and C2M2G mice that are heterozygous for the transgenic allele do also reliably indicate microglial Ca<sup>2+</sup> level changes, we only used homozygous indicator mice in the present study.

### Immunohistochemistry and confocal microscopy

Mice were anesthetized with pentobarbital (Narcoren, Merial Hallbergmoos, Germany) and transcardially perfused with 0.9% NaCl followed by 4% paraformaldehyde in 0.1 M phosphate buffer (PB), decapitated and sectioned in the sagittal plane at 40 μm thickness, using a sliding microtome (Leica SM2000 R, Leica Biosystems GmbH, Nussloch, Germany). The brain slices were stored in CPS solution (Glycerin + Ethylenglykol) at –20°C until further use. For immunohistochemical stainings, free-floating 40 μm sections were incubated 1h with 5% donkey serum (EMD Millipore Corp., Burlington, Massachusetts, USA) and 0.1% Triton-X (Carl Roth®, Karlsruhe, Germany) in Tris-buffered saline solution (TBS) and after with the primary antibodies in 5% donkey serum in TBS, over-night at 4°C. The following primary antibodies were used: goat monoclonal Iba-1 antibody targeting microglia (1:400; Abcam, Cambridge, UK); chicken polyclonal GFP antibody targeting GCaMP6m (1:250; Abcam, Cambridge, UK); rabbit anti-RFP targeting the mCherry protein (1:200; Rockland Immunochemicals, Limerick, PA, USA); polyclonal guinea pig anti-GABA (1:500; Abcam, Cambridge, UK); anti-NeuN targeting neurons (1:100; Synaptic Systems) and polyclonal rabbit anti-gabbr1 (1:150; Chemicon international, California) and guinea pig polyclonal anti-GFAP (1:500; Synaptic Systems) for targeting astrocytes. After washing, secondary antibodies were prepared in TBSplus. Iba-1 was visualized with donkey anti-goat IgG conjugated with Cy5 fluorophore (1:200; Dianova, Hamburg, Germany); GFP was visualized with donkey anti-chicken IgY conjugated with Alexa488 (1:200; Dianova), the RFP with donkey anti-rabbit IgG (H+L) conjugated with Cy3 (1:200; Dianova), GABA with donkey anti-guinea pig IgG (H+L) conjugated with Cy5 (1:150; Dianova, Hamburg, Germany), NeuN with donkey anti-mouse IgG (H+L) conjugated with Cy3 (1:200; Dianova), gabbr1 with donkey anti-rabbit IgG (H+L) conjugated with Cy3 (1:200; Dianova) and GFAP with donkey anti-rabbit IgG (H+L) conjugated with Cy3 (1:200; Dianova) or donkey anti-guinea pig IgG (H+L) conjugated with Dylight 405 (1:500; Thermo Fisher Scientific). The slices were then mounted on glass slides with Aqua Poly-mount mounting medium (Polysciences Europe GmbH, Hirschberg an der Bergstraße, Germany). Cell nuclei were stained using 4',6-diamidino-2-phenylindole (DAPI, 1:500; Dianova) and sections were incubated with secondary antibodies at room temperature for 2h. Images were acquired with a Leica SPE (Leica Microsystems GmbH, Nussloch, Germany) using a 10X (C PLAN 10.0x0.22 POL HCX PLAPO C5) and a 63X (63x1.20 W CORR UV) objective. Z stacks were taken at 1 μm Z-step size, 25–42 steps to cover at least one layer of microglia (10–14 brain slices/animal with n = 3 animals/group).

### Acute brain slice preparation

Acute brain slices were prepared as previously described (Boucsein et al., 2003) from adult (P45–70), juvenile (P13–14) and neonatal (P5–6) C2G and C2M2G mice. Briefly, after cervical dislocation, mice were decapitated and the brains were immediately extracted and placed in ice-cold solution, saturated with carbogen (95% O<sub>2</sub>, 5% CO<sub>2</sub>) and containing (in mM): 230 sucrose, 26 NaHCO<sub>3</sub>, 2.5 KCl, 1.25 NaH<sub>2</sub>PO<sub>4</sub>, 10 MgSO<sub>4</sub>(7H<sub>2</sub>O), 0.5 CaCl<sub>2</sub>(2H<sub>2</sub>O) and 10 glucose. The cerebellum and the olfactory bulbs were gently removed. Coronal slices with a thickness of 270 μm were generated using a vibratome (HM650V, Thermo Scientific, Massachusetts, USA) and placed at room temperature in artificial cerebrospinal fluid (ACSF) containing (in mM): 134 NaCl; 26 NaHCO<sub>3</sub>; 2.5 KCl; 1.26 K<sub>2</sub>HPO<sub>4</sub>; 1.3 MgCl<sub>2</sub>(6H<sub>2</sub>O); 2 CaCl<sub>2</sub>(H<sub>2</sub>O) and 10 D-glucose; pH 7.4, gassed with carbogen (95% O<sub>2</sub>/ 5% CO<sub>2</sub>). The brain slices were kept in aCSF until further treatment.

### *In situ* Ca<sup>2+</sup> imaging

Ca<sup>2+</sup> imaging experiments were performed 1–5h after the slicing procedure at room temperature. Brain slices were placed into the recording chamber which was constantly perfused with carbogenized (95% O<sub>2</sub>, 5% CO<sub>2</sub>) ACSF by a perfusion pencil which was used for the local application of the tested substances as well as of 1 mM ATP (Adenosine-3-Phosphate) which was applied at the end of every recording as control. The perfusion speed was adjusted to 0.5 ml/min.

For epifluorescence imaging, we used an AxioScope 2 FS plus (Carl Zeiss Microscopy GmbH, Jena, Germany) which was equipped with 10X and 40X water immersion objectives. The GCaMP6m protein was excited by a Polychrome IV (Till Photonics, Gräfeling, Germany) or an HBO-100 lamp. Excitation (470–490 nm) and emission wavelengths (510–550 nm) were filtered using appropriate optical filter sets. The 10x objective was used for the localization of the interested brain region and the 40x was used for most Ca<sup>2+</sup> imaging recordings. Movies were taken at a frequency of 1 frame/sec by a Zyla 5.5 camera (Oxford Instruments, Belfast, UK) driven by Solis software. Amplifier (EPC 9 or EPC10, HEKA Electronics, Lamprecht, Germany) and TIDA 5.25 (HEKA Electronics) were used to trigger fluorescence excitation and image acquisition.

For 2-Photon imaging, we used a custom-built 2-photon microscope consisting of an BX61WI microscope stage (Olympus, Hamburg, Germany) equipped with 10x water immersion objective placed on a PD72Z4CA piezo drive (Physik Instrumente, Karlsruhe, Germany), a Chameleon Ultra II laser (Coherent, Dieburg, Germany) and GaAsP photomultipliers (Thorlabs, Lübeck, Germany). The GCaMP6m protein was excited at a wavelength of 940 nm. Movies were acquired at a sampling rate of one 3D image per second. Each 3D image covered seven z-planes at 7  $\mu\text{m}$  distance and an area of 640  $\mu\text{m}$   $\times$  640  $\mu\text{m}$ . ThorImage 8.0 was used to drive the image acquisition during  $\text{Ca}^{2+}$  imaging experiments.

The acquisition of the mCherry and GCaMP6m fluorescence signals in microglia was performed at the confocal laser scanning microscope Zeiss LSM 880 with AxioExaminerZ1 (Carl Zeiss Microscopy GmbH, Jena, Germany). Z stacks of microglial soma and processes were imaged with a PlanApo 20x NA 1.0 water dipping objective, driven by a piezo driver on the z axis and scanning a total area of 304  $\mu\text{m}$   $\times$  135  $\mu\text{m}$  with a pixel size of 0.42  $\mu\text{m}$  laterally and 2  $\mu\text{m}$  axially for 12  $\mu\text{m}$  (PH setting 1.7 AU) at 16 bit. The mCherry and GCaMP6m proteins were simultaneous excited with the 488 nm and 561 nm lasers and detected at 500–550 nm (GaAsP) and 595–650 nm (PMT), respectively using bidirectional scanning at scan speed 9 to achieve a high frame rate. Note, only microglial cells in CA1 and more distant than 300  $\mu\text{m}$  from the stimulation were recorded. Transmitted light images were recorded to locate the pipettes. The Zen 2.3 SP1 software was used to set and drive the image acquisition.

For offline analysis, each 3D image in the  $\text{Ca}^{2+}$  recordings from the 2-photon or the LSM880 was subjected to a maximum intensity projection to obtain a 2D movie by using a custom-built procedure in IGOR Pro 6.37 (WaveMetrics, Lake Oswego, USA) or Fiji ImageJ (NIH), respectively.

### Electrical stimulation

Excitatory field potentials were recorded at room temperature in freshly prepared brain slices that were placed in a recording chamber mounted on an upright 2-photon microscope (see above). Stimulation and recording electrodes (impedance 1 MOhm) were placed in the hippocampal regions CA3 and CA1, respectively. The two electrodes were between 410–560  $\mu\text{m}$  apart. fEPSPs were reliably obtained by the application of a single train of 100 pulses at a frequency of 100 Hz. Amplifier (EPC9 or EPC10, HEKA Electronics) and TIDA 5.25 (Heka electronics) were used to apply the electrical stimulation and to record the postsynaptic potentials.

## QUANTIFICATION AND STATISTICAL ANALYSIS

### Quantification of immunohistochemical stainings

*Gabbr1* signals in microglia (Figures 4C, 4D, 6D, and 6E) were quantified from 8bit 3D images using a custom-built procedure in IGOR Pro 6.37 (WaveMetrics; see Methods S1, program codes 3. and 4.). Briefly, a prismatic volume of interest (VOI) was manually set over a perisomatic region of a microglia. Voxels were binarized into Iba1<sup>+</sup> (intracellular) and Iba1-negative (extracellular) after Gaussian filtering (N = 3) by a constant threshold which was 30 AU for all analyzed cells in our analysis. Binarized DAPI signals (threshold = 50 AU) were used to exclude the nuclear part of the intracellular volume. Subsequently, the threshold for GABA<sub>B</sub>R was determined as mean+2\*SD from all extracellular *Gabbr1* signals. This means that the *Gabbr1* threshold value was individual for each analyzed cell. A microglia was counted as *Gabbr1*<sup>+</sup> when more then 5% of the intracellular voxels were above the calculated *Gabbr1* threshold.

Analysis of GABA signals in astrocytes was also performed on 3D confocal SPE images (8bit). A prismatic volume of interest (VOI) was manually set over a perisomatic region of an astrocyte. Voxels were binarized into *Gfap*<sup>+</sup> (intracellular) and *Gfap*-negative (extracellular) after Gaussian filtering (N = 3) by a constant threshold which was 30 AU for all analyzed cells. GABA levels were subsequently calculated as mean fluorescence values of the intracellular voxels in the GABA channel. We applied a Mann-Whitney U test test to calculate significance levels between data sets. Data are given as median  $\pm$  25%/75% percentile. Statistical significance levels are represented as n.s.:  $p > 0.05$ ; \*:  $p < 0.05$ ; \*\*:  $p < 0.01$ ; \*\*\*:  $p < 0.001$ .

### Data analysis of $\text{Ca}^{2+}$ imaging movies

$\text{Ca}^{2+}$  imaging movies were analyzed using a home-made algorithm in Igor Pro 6.37 (WaveMetrics; see Methods S1, program codes 1. and 2.). For analysis, cell somata which were visible in the presence of ATP at the end of each experiment were selected as ROIs, and the mean relative fluorescent intensity for each ROI and frame was determined to display changes in  $\text{Ca}^{2+}$  levels for each cell. Therefore, only ATP-responding microglia were taken into the subsequent analysis. Intracellular  $\text{Ca}^{2+}$  elevations were counted as “responsive” (agonist or electrical stimulation) when microglial  $\text{Ca}^{2+}$  response amplitudes exceeded four times the SD of the baseline. We averaged the responses from each slice to obtain one “n” for the subsequent statistics. For the analysis of amplitudes and kinetics of microglial  $\text{Ca}^{2+}$  responses, we used all “responding” events and excluded non-responders.

Igor Pro 6.37 (WaveMetrics) and Prism 7 (GraphPad Software, San Diego, CA, USA) were used for statistical analysis. Statistical significance levels were represented as \* $p \leq 0.05$ ; \*\* $p \leq 0.01$ ; \*\*\* $p \leq 0.001$ . Data are expressed as mean  $\pm$  SEM.